APEM
journal

Advances in Production Engineering & Management

University of Maribor

Advances in Production Engineering & Management

Identification Statement

APEM Editorial

Advances in Production Engineering & Management

Contents

Scope and topics

Advances in Production Engineering & Management (*APEM journal*) is an interdisciplinary refereed international academic journal published quarterly by the *Production Engineering Institute* at the *University of Maribor*. The main goal of the *APEM journal* is to present original, high quality, theoretical and application-oriented research developments in all areas of production engineering and production management to a broad audience of academics and practitioners. In order to bridge the gap between theory and practice, applications based on advanced theory and case studies are particularly welcome. For theoretical papers, their originality and research contributions are the main factors in the evaluation process. General approaches, formalisms, algorithms or techniques should be illustrated with significant applications that demonstrate their applicability to real-world problems. Although the *APEM journal* main goal is to publish original research papers, review articles and professional papers are occasionally published.

Fields of interest include, but are not limited to:

Additive Manufacturing Processes	Machine Tools
Advanced Production Technologies	Machining Systems
Artificial Intelligence	Manufacturing Systems
Assembly Systems	Mechanical Engineering
Automation	Mechatronics
Cutting and Forming Processes	Metrology
Decision Support Systems	Modelling and Simulation
Discrete Systems and Methodology	Numerical Techniques
e-Manufacturing	Operations Research
Fuzzy Systems	Operations Planning, Scheduling and Control
Human Factor Engineering, Ergonomics	Optimisation Techniques
Industrial Engineering	Project Management
Industrial Processes	Quality Management
Industrial Robotics	Queuing Systems
Intelligent Systems	Risk and Uncertainty
Inventory Management	Self-Organizing Systems
Joining Processes	Statistical Methods
Knowledge Management	Supply Chain Management
Logistics	Virtual Reality

Frictional characterization of teak wood dust-filled epoxy composites

Mishra, A.[a,*]

[a]Indira Gandhi Institute of Technology, Sarang, Odisha, India

ABSTRACT

Composites of teak wood dust particles of 150 μm, 212 μm, and 300 μm sizes with 10 % weight fractions were developed by a hand moulding technique. A wooden mould was prepared for casting the composite pins of 8 mm diameters and 50 mm length. Sliding wear tests were conducted on a pin on disc friction and wear monitor. It was observed that the composite with mesh size 150 μm of teak wood dust exhibited the least wear rate. Furthermore, the lowest coefficient of friction was also seen in the composite with a 300 μm size wood dust filler. The composite with 212 μm size wood dust showed an increase in the coefficient of friction but at higher loads dropped down probably because of the formation of transfer film between the composite and the steel disc. The composites with 150 μm and 300 μm size dust particles were in close ranges of friction coefficients, i.e. 0.64 and 0.71, respectively. Thus though the coefficient of friction was high for a 150 μm size filler composite, the wear increased at a steady rate and may stabilize after running for more than a 5 km distance later. Out of the above three composites the wood dust of a 150 μm composite may thus be a better choice for frictional applications.

1. Introduction

The quest for light weight and high strength materials is never ending for due consideration owing to their wide applications. Therefore a polymeric composite material has its importance in the applications of light structures. These composite materials (notably aramid, carbon and glass fibre reinforced plastics etc.) now dominate the aerospace, automotive, construction, and sporting industries. However, these fibres have serious drawbacks such as non-renewability, non-recyclability, non-bio-degradability etc. These shortcomings have been highly exploited by proponents of natural fibre composites. Though mechanical properties of natural fibres are much inferior to those of other fibres, their specific properties, especially stiffness, are quite comparable to artificial fibres.

The aim of this study is to determine the friction and wear characteristics of saw dust-epoxy composite. This study is important for thermoplastic manufacture of furniture, residential deck board, rails and balusters, transportation structures, poles and cross arm, wearing surfaces and other related industrial applications to find out suitable materials which show good friction and wear properties.

Although there are several reports in the literature which discuss the mechanical behaviour of wood/polymer composites, however, very limited work has been done on the effect of wood dust types on friction and wear characteristics of polymer composites. Against this background,

the present research work has been undertaken, with an objective to explore the potential of wood dust types as a reinforcing material in polymer composites and to investigate its effect on the friction and wear behaviour of the resulting composites. Most of the studies on natural fibre composites involve study of mechanical properties as a function of fibre content, effect of various treatments of fibres, and the use of external coupling agents. In the literatures, many works devoted to the properties of natural fibres from micro- to nano-scales are available. A number of investigations have been conducted on several types of natural fibres such as kenaf, hemp, flax, bamboo, and jute to study the effect of these fibres on the mechanical properties of composite materials. Mansur and Aziz [1] studied bamboo-mesh reinforced cement composites, and found that this reinforcing material could enhance the ductility and toughness of the cement matrix, and increase significantly its tensile, flexural, and impact strengths. Fracture properties and characteristics of sisal textile reinforced epoxy composites were studied by Li et al. [2]. The study concluded that proper fibre surface treatment could improve the fracture properties of this kind of eco-composite. Mechanical and fracture properties of Australian bamboo was studied by Low et al. [3]. It investigated the microstructure, mechanical, impact and fracture properties. Mosadeghzad et al. [4] studied the effect of surface treatment and filler loading on mechanical properties of the acacia saw dust unsaturated polyester resin (UPR) composite based on recycled polyethylene-terephthalate (PETP). The results showed that both tensile and flexural moduli were increased with increasing filler contents whereas the strength was decreased. This was overcome by treating the sawdust fillers with 10 % sodium hydroxide (NaOH). Study on the wear-resisting property of wood Cu/Ni electroplate coating was done by Huang et al. [5] which showed that the treated metal-wood surface has higher wear-resisting property and hardness. Biswas et al. [6] worked on the effect of ceramic fillers on mechanical properties of bamboo fibre reinforced epoxy composites. In this study, a series of bamboo fibre reinforced epoxy composites were fabricated using conventional filler (aluminium oxide Al_2O_3) and silicon carbide (SiC) and industrial wastes (red mud and copper slag) particles as filler materials. The result showed that the inclusion of fibre in neat epoxy improved the load bearing capacity (tensile strength) and the ability to withstand bending (flexural strength) of the composites. Kranthi et al. [7] studied the wear performance of a new class of epoxy based composites filled with pine wood dust. According to the study pine wood dust possesses good filler characteristics as it improves the sliding wear resistance of polymeric resin, and filler content, sliding velocity and normal loads are the important factors which affect the specific wear rate. A comparison of properties between glass-epoxy-fly ash and fly ash-epoxy composite has been made by Singla and Chawla [8]. Compression and impact tests have been carried out with varying weight fractions of fly ash and glass reinforcements in epoxy. SEM has been done to analyze the fractured surfaces. Chemical resistance to acids, alkalis and solvents to jute-glass and varying weight fractions of silica filled composites have been analzed by Kumar and Madhu [9]. It was concluded that all the composites have shown better chemical resistance to acids and alkalis except to toluene. A study on the dry sliding wear of oil palm empty fruit bunch (OPEFB) epoxy composite was done by Kasolang et al. [10]. The result showed that the mass loss was significantly higher for smallest fibre size (100 μm) examined at 30 N and at other fibre sizes, the mass loss values were relatively close due to the distribution and orientation of fibres. Wang et al. [11] studied the effect of coupling agent on bonding properties of wood/polyethylene composites. The result showed that the -OH, -C-O- and C=O functional groups were appeared on the treated surface and the surface roughness was increased after mechanical polishing treatment and coating treatment, resulting increase in the shear bonding strength for the treated sample significantly. Hisham et al. [12] studied the flexural mechanical characteristic of sawdust and chip wood filled epoxy composites and found that a good quality of saw wood (SW) and chip wood (CW) fibre composite can be used for furniture utilities. Nagieb et al. [13] investigated the effect of addition of boric acid and borax on fire-retardant properties and studied the mechanical properties of urea formaldehyde saw dust composites. The experimental results showed that the water absorption and bending strength decreased as the flame retardant increased. A study on the microstructures and properties of wood ceramics prepared from bagasse and epoxy resin composite was done by Zhang et al. [14]. The carbon yield ratio of the wood ceramics decreased with the increase of the content of ba-

gasse. While the volume shrinkage ratio and volume electrical resistivity increased with the increase of the content of bagasse. Wimonsong et al. [15] worked on thermal conductivity and mechanical properties of wood sawdust/polycarbonate composites. The study showed that the Young's moduli of composites were in general higher than the neat PC except for the one with γ-aminopropyl trimethoxy silane treatment. The tensile moduli of composites were increased as the filler loading increased and the addition of wood sawdust resulted in the tensile strength reduction of the composites, and also the thermal conductivity was reduced significantly with the increment of wood sawdust contents. Girisha et al. [16] have studied the mechanical performance of natural fibre reinforced (treated and untreated) hybrid composites. Tamarind fruit fibre and arecanut fibres were reinforced to epoxy. For treated fibres it was observed that tensile strength and flexural strength have increased with increase in fibre volume fractions. However beyond 40 % reinforcement the strength has decreased. Impact properties of 50 % reinforced composite has yielded the best result. Bhaskar et al. [17] worked on the evaluation of properties of polypropylene-pine wood plastic composite. Incorporation of maleated polypropylene (MAPP) coupling agent in composite formulation improved the stability. Vafaeneezhad et al. [18] considered carbonized wood from oak tree to prepare carbon/epoxy composites. From experiments it was observed that addition of epoxy has increased the sliding wear resistance. Artificial neural network was developed to validate the experimental findings. It was found that sliding distance, normal load and carbonization temperature played important role affecting the wear characteristics of the composite. Coir dust with 10 %, 20 %, and 30 % concentration both treated and untreated types were tested by Chandra Rao et al. [19] on a pin on disc type friction monitor. In order to minimize the experimental time and cost, Taguchi method was used. Abrasive wear characteristics were studied with varying load up to 30 N and varying velocities. It was seen that treated filler composites showed better wear resistance compared to untreated ones. With increase in dust content the wear rate decreased but with increase in load the wear rate has increased. Mishra [20] investigated the friction and wear characteristics of teak wood dust-filled epoxy composites of three different types of specimens. It was observed that wood dust-filled with 10 % of 300 μm size composite has exhibited better wear performance.

Thus out of the above review an attempt has been made in this investigation to:

- Development of teak wood dust-filled epoxy composites with different mesh sizes and constant volume fraction (10 % by weight).
- Casting of cylindrical pins of 8 mm diameter for frictional characterization by developing a suitable wooden mould.
- Carrying out short run and long run tests in a pin on disc friction and wear monitor to evaluate the coefficient of friction and wear characteristics of these materials sliding against mild steel plate.
- Choosing the best out of the above three specimens for specific application.

This paper describes the calculation of mechanical properties of the composite as applied to random distributed particle reinforced composites along with weight fractions and volume fractions of the reinforcement, development of a suitable mould for casting composite pins, experimental work carried out on a pin on disc machine for determining the coefficient of friction and wear rate. Lastly the results obtained have been discussed and conclusions have been drawn out of the findings. Recommendations have also been made for expected applications of these composites.

2. Mechanical properties of the composite

The composite is usually prepared based on calculation of weight fractions or volume fractions. Weight fraction of the reinforcement:

$$w_r = \frac{W_r}{W_r + W_m} \cdot 100 \qquad (1)$$

Weight fraction of the matrix is:

$$w_m = \frac{W_m}{W_r + W_m} \cdot 100 \tag{2}$$

where W_r is weight of reinforcement, and W_m weight of the matrix. Weight of the composite is:

$$W_c = W_r + W_m \tag{3}$$

Further as per rule of mixtures, the density of the composite ρ_c is obtained by:

$$\rho_c = \rho_m \cdot v_m + \rho_r \cdot v_r \tag{4}$$

where ρ_m is density of the matrix, ρ_r is density of the reinforcement, v_m is volume fraction of the matrix, and v_r is volume fraction of the reinforcement. Further:

$$v_m = \frac{V_m}{V_m + V_r + V_v} \cdot 100 \tag{5}$$

and

$$v_r = \frac{V_r}{V_m + V_r + V_v} \cdot 100 \tag{6}$$

Volume of the composite is:

$$V_c = V_m + V_r + V_v \tag{7}$$

where V_m is volume of the matrix, V_r is volume of the reinforcement and V_v is volume of voids. Modulus of elasticity of the composite is:

$$E_c = E_r \cdot v_r + E_m \cdot v_m \tag{8}$$

where E_r is modulus of elasticity of reinforcement and E_m is modulus of elasticity of matrix.

The properties of teak wood dust and epoxy are shown in the Table 1 and Table 2, respectively. By using the Eq. 4 and Eq. 8 the density and elastic modulus of the composites have been found out and given in Table 3.

Table 1 Properties of teak wood dust [20]

Properties	Value
Density (g/cm³)	0.8
Young's modulus of elasticity (GPa)	10.5
Tensile strength (MPa)	95

Table 2 Properties of epoxy [20]

Properties	Value
Density (g/cm³)	1.2*10³
Young's modulus of elasticity (GPa)	20
Tensile strength (MPa)	75

Table 3 Composite properties

Specimens	Density (kg/m³)	Elastic modulus (GPa)
Sp-1 (300 µm)	1120	18.58
Sp-2 (212 µm)	1140	18.58
Sp-3 (150 µm)	1160	19.05

3. Experimental investigations

3.1 Materials

The teak wood dust of different sizes, i.e. 150 μm, 212 μm, and 300 μm (Fig. 1) measured through sieve shaker were considered as reinforcing material (10 % by weight) in fabrication of the composite. Epoxy (CY 230 and Hardener-HY-951 supplied by Hindustan Ceiba Geigy, Ltd.) has been used as matrix material. A wooden mould has been developed in house to cast the pins for wear testing (Fig. 2). After mixing epoxy and wood dust in the proposed ratio the composite was cast by pouring into the split mould and allowed to cure at room temperature for 24 hours. The pins were ejected out after solidification (Fig. 3).

Fig. 1 Teak wood dust of three sizes: 150 μm (left), 212 μm (center), and 300 μm (right)
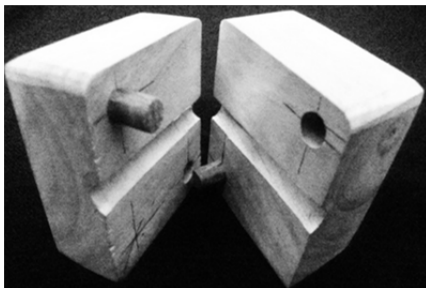
Fig. 2 Wooden mould for pins

Fig. 3 Composite pins (150 μm, 212 μm, and 300 μm)

3.2 Experimental procedure

The tests were carried out in pin on disc wear and friction testing machine (Fig. 4 and Fig. 5) supplied by M/s Magnum Engineers, Bangalore, India, having the following specifications:

- Load range: up to 100 N,
- Friction force measurement: up to 100 N,
- Wear measurement: 2000 μm (± 2 mm),
- Sliding speed: 0.26-10.0 m/s,
- Disc speed: 100-2000 rpm,
- Diameter of track: 40-90 mm,
- Disc size: diameter is 100 mm and thickness is 8 mm, disc material is EN-31 (58-60 RC),
- Pin: diameter is 3-10 mm and length is 25 mm,
- Software: MAGVIEW-2011 data acquisition software.

For evaluation of friction coefficient under dry sliding condition the speed and time were kept constant, i.e. 400 rpm and 3 min with varying the load up to 5 kg. Similarly for estimating the wear, the pins were slid against mild steel disc for 5 km of sliding distance keeping the speed at 400 rpm (1.5 m/s sliding velocity) and load of 30 N.
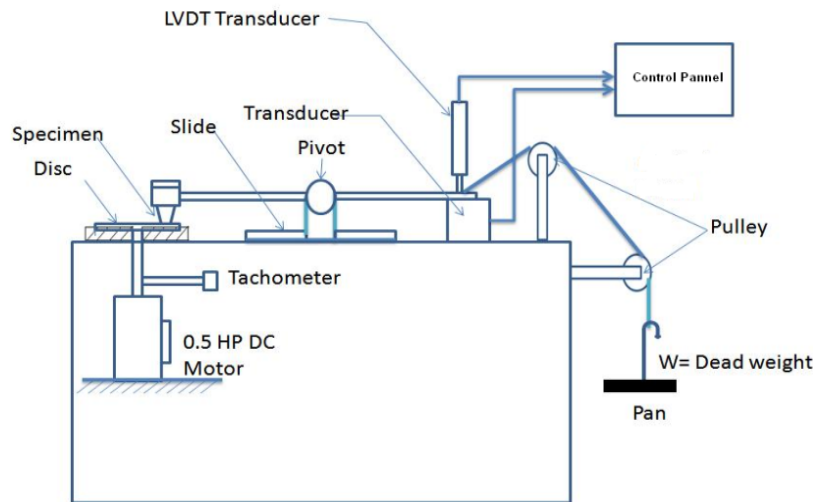
Fig. 4 A schematic diagram of the pin on disc apparatus

Fig. 5 Friction and wear monitor [20]

4. Results and discussions

The readings from the control panel of the pin on disc apparatus with respect to friction force, speed, wear, and time have been taken during conduct of the wear tests. The dead weights placed on the apparatus gave direct measurement of the normal reaction. Hence the coefficient of friction could be calculated. Thus the coefficient of friction and wear in microns were obtained for three different specimens (Table 4 and Table 5):

- Specimen-1: composite with teak wood dust of 300 μm,
- Specimen-2: composite with teak wood dust of 212 μm,
- Specimen-3: composite with teak wood dust of 150 μm.

The results have also been plotted graphically to give a better understanding as shown in Fig. 6 and Fig. 7.

Table 4 Variation of coefficient of friction with load

Load (kg)	Specimen-1	Specimen-2	Specimen-3
1	0.52870	0.468700	0.43388
2	0.55750	0.559700	0.51084
3	0.59248	0.694020	0.57949
4	0.62229	0.843042	0.64327
5	0.63915	0.872820	0.71206

Table 5 Variation of wear with sliding distance

Load (kg)	Specimen-1	Specimen-2	Specimen-3
1	71.4830	33.7410	1.4080
2	72.6330	100.907	41.286
3	79.1380	145.524	79.797
4	89.0808	162.124	169.192
5	104.932	175.803	241.926
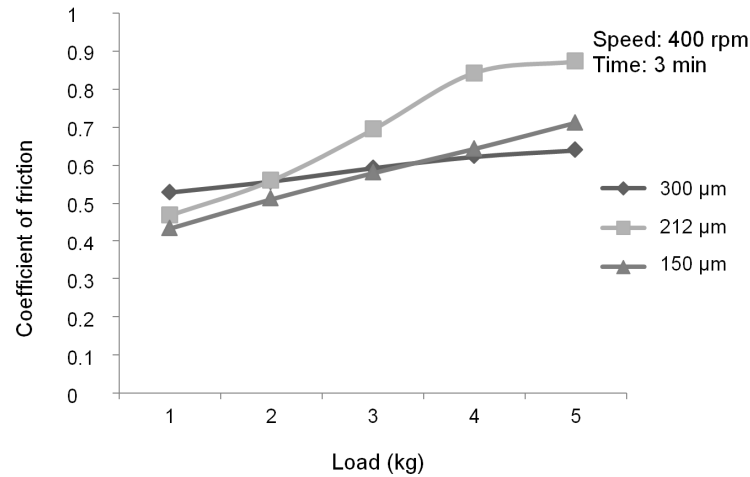
Fig. 6 Variation of coefficient of friction against load
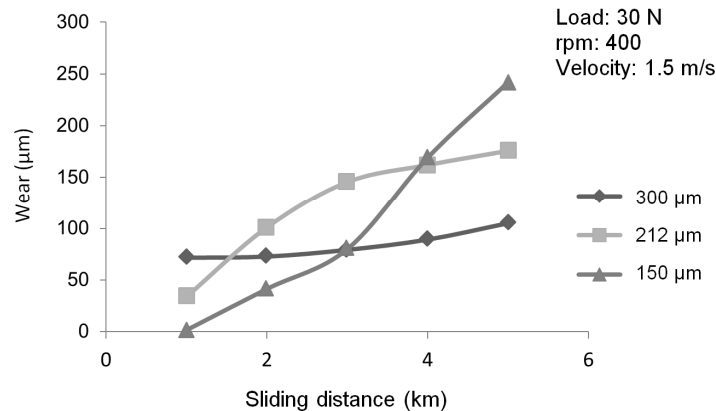
Fig. 7 Variation of wear with sliding distance

Out of the above results it is observed that the composite with mesh size 150 μm of teak wood dust exhibited least wear rate. Further lowest coefficient of friction has also been seen in the composite with 300 μm size wood dust filler. The composite with 212 μm size wood dust showed increase in coefficient of friction and at higher loads it may drop down probably because of formation of transfer film between the composite pin and the steel disc. The composites with 150 μm and 300 μm size dust particles are in close range of coefficient of friction, i.e. 0.64 and 0.71, respectively.

5. Conclusion

From the theoretical investigations it is revealed that composite with teak dust of 150 μm size has highest modulus of elasticity and density obtained by rule of mixtures. Further the co efficient of friction is also high for 150 μm size filler composite with least wear as compared to others. However it is observed that wear increases at a steady rate which may stabilize after run-

ning for more than 5 km distance. Out of the above three composites thus the wood dust of 150 μm composite is a better choice for frictional applications. This type of composites can be used as packing materials, interior decoration of houses and buildings, light weight furniture, aircrafts interiors and automobile components etc. Long run wear tests are to be carried out for ascertaining its application in high frictional environment in industries.

Acknowledgement

References

[1] Mansur, M.A, Aziz, M.A. (1983). Study of bamboo-mesh reinforced cement composites, *International Journal of Cement Composites and Lightweight Concrete*, Vol. 5, No. 3, 165-171, doi: 10.1016/0262-5075(83)90003-9.

[2] Li, Y., Mai, Y.W., Ye, L. (2006). Fracture properties and characteristics of sisal textile reinforced epoxy composites, *Key Engineering Materials,* Vol. 312, 167-172, doi: 10.4028/www.scientific.net/KEM.312.167.

[3] Low, I.M., Che, Z.Y., Latella, B.A., Sim, K.S. (2006). Mechanical and fracture properties of bamboo, *Key Engineering Materials,* Vol. 312, 15-20, doi: 10.4028/www.scientific.net/KEM.312.15.

[4] Mosadeghzad, Z., Ahmad, I., Daik, R., Ramli, A., Jalaludin, Z. (2009). Preparation and properties of acacia sawdust/UPR composite based on recycled PET, *Malaysian Polymer Journal*, Vol. 4, No. 1, 30-41.

[5] Huang, J.T., Jia, J. Tie, K.L. (2010). Study on the wear-resisting property of wood Cu/Ni electroplate coating, *Advanced Materials Research,* Vol. 123-125, 1055-1058, doi: 10.4028/www.scientific.net/AMR.123-125.1055.

[6] Biswas, S., Satapathy, A., Patnaik, A. (2010). Effect of ceramic fillers on mechanical properties of bamboo fiber reinforced epoxy composites: a comparative study, *Advanced Materials Research,* Vol. 123-125, 1031-1034, doi: 10.4028/www.scientific.net/AMR.123-125.1031.

[7] Kranthi, G., Nayak, R., Biswas, S., Satapathy, A. (2010). Wear performance evaluation of pine wood dust filled epoxy composites, In: *Proceedings of the International Conference on Advancements in Polymeric Materials APM*, National Institute of Technology, Rourkela, India, 1-5.

[8] Singla, M., Chawla, V. (2010). Mechanical properties of epoxy resin – fly ash composites, *Journal of Minerals & Materials Characterization and Engineering,* Vol. 9, No. 3, 199-210.

[9] Kumar, M.A., Madhu, K. (2011). Improvement of chemical resistance of silica/epoxy/hybrid (jute/glass) fibre composites, *International Journal of Macromolecular Science*, Vol. 1, No. 1, 23-25.

[10] Kasolang, S., Kalam, A., Ahmad, M.A. (2011). Dry sliding wear of oil palm empty fruit bunch (OPEFB) epoxy composite, *Advanced Materials Research,* Vol. 308-310, 1535-1539, doi: 10.4028/www.scientific.net/AMR.308-310.1535.

[11] Wang, H., Lv, X.Y., Di, M.W. (2011). Effect of coupling agent on bonding properties of wood/polyethylene composites, *Advanced Materials Research,* Vol. 311-313, 59-62, doi: 10.4028/www.scientific.net/AMR.311-313.59.

[12] Hisham, S., Faieza, A.A., Ismail, N., Sapuan, S.M., Ibrahim, M.S. (2011). Flexural mechanical characteristic of sawdust and chip wood filled epoxy composites, *Key Engineering Materials,* Vol. 471-472, 1064-1069, doi: 10.4028/www. scientific.net/KEM.471-472.1064.

[13] Nagieb, Z.A., Nassar, M.A., El-Meligy, M.G. (2011). Effect of addition of boric acid and borax on fire-retardant and mechanical properties of urea formaldehyde saw dust composites, *International Journal of Carbohydrate Chemistry,* Vol. 2011, 1-6, doi: 10.1155/2011/146763.

[14] Zhang, C.H., Pan, J.M., Yan, X.H., Cheng, X.N., Xu, G.F., Gao, Y.Q. (2011). Microstructures and properties of woodceramics prepared from bagasse and epoxy resin composite, *Advanced Materials Research,* Vol. 412, 402-405, doi: 10.4028/www.scientific.net/AMR.412.402.

[15] Wimonsong, W., Threepopnatkul, P., Kulsetthanchalee, C. (2012). Thermal conductivity and mechanical properties of wood sawdust/polycarbonate composites, *Materials Science Forum,* Vol. 714, 139-146, doi: 10.4028/ www.scientific.net/MSF.714.139.

[16] Girisha, C., Murthy, S., Rangasrinivas, G., Manu, S. (2012). Mechanical performance of natural fibre reinforced epoxy hybrid composites, *International Journal of Engineering Research and Applications*, Vol. 2, No. 5, 615-619.

[17] Bhaskar, J., Haq, S., Pandey, A.K., Srivastava, N. (2012). Evaluation of properties of propylene–pine wood plastic composite, *Journal of Materials and Environmental Science,* Vol. 3, No. 3, 605-612.

[18] Vafaeenezhad, H., Zebarjad, S.M., Khaki, J.V. (2012). Fabrication and wear behaviour of the carbon/epoxy composites based on wood using artificial neural networks, *Advanced Materials Research,* Vol. 413, 95-102, doi: 10.4028/www.scientific.net/AMR.413.95.

[19] Chandra Rao, C.H., Madhusudan, S., Raghavendra, G., Venkateswara Rao, E. (2012). Investigations into wear behavior of coir fiber reinforced epoxy composites with the Taguchi method*, International Journal of Engineering Research and Applications*, Vol. 2, No. 5, 371-374.

[20] Mishra, A. (2014). Investigations on wear characteristics of teak wood dust filled epoxy composites, *Journal of Production Engineering,* Vol. 17, No. 1, 75-78.

Optimal fractal dimension on grain structure robot laser-hardened tool steel

Babic, M.[a,*], **Balic, J.**[b], **Kokol, P.**[c]

[a]EMO-Orodjarna d.o.o., Celje, Slovenia
[b]Faculty of Mechanical Engineering, University of Maribor, Slovenia
[c]Faculty of Electrical Engineering and Computer Science, University of Maribor, Slovenia

ABSTRACT

In order to optimize the structure and properties of tool steel, it is necessary to take into account the effect of the self-organization of a dissipative structure with fractal properties at load. Fractal material science researches the relationship between the parameters of fractal structures and the dissipative properties of tool steel. This paper describes the application of fractal dimension in robot laser-hardening specimens. By using fractal dimensions, changes in the structure can be determined because the fractal dimension is a present indicator of the complexities of the sample forms. We hardened tool steel at different speeds and different temperatures. By researching the fractal dimensions of the microstructures of the hardened specimens we could better understand the effects of the parameters of robot cells on the material. We show the experimental results and an analysis of those fractal patterns that occur during robot laser hardening with the different parameters of temperature and speed. Finally, we present the relationship between the fractal dimensions and the parameters of temperature and speed of robot laser hardening. The hardening of various metal alloys showed that when melting occurs, fractal geometry can be used to calculate the fractal dimension. The dependence of the fractal dimension on the hardness was ascertained. This finding is important when we realize that certain alloys mix poorly because they have different melting temperatures but such alloys have a much higher hardness and better technical characteristics.

1. Introduction

Of all microscopic methods, electron microscopy images give the best resolution, the most accurate information of the distribution of crystals in a building, the best morphology of the various structural types, and the best structural surface topography. Fractal geometry provides a new approach in describing the structure of various illegal structures. Fractal theory has also been used in the field of materials science. Models of fractal lines and surfaces were created to describe the properties of the microstructure of materials [1]. The subject of fractals can be used to assist in the analysis of surfaces encountered in robot laser hardening. It should be noted that the morphology of a surface will change if material is hardened with robot laser cells. Analysis of fractal dimensions is a method used to study the surface properties of materials. Fractal dimension [2] is a property of fractals that is maintained over all magnifications and is therefore well defined, but in addition, it also reveals the complexity of the fractal. In general, we cannot calculate the fractal dimension for the above-mentioned procedure, as this is possible only on pure

mathematical constructs, and not by nature. In practical terms, to determine the dimensions the most used method is that "of counting boxes" (box-counting dimension), which studies fractal cover using a square grid, which is then reduced and the change in the number of squares needed to cover the entire crowd observed. We face many problems in robot laser hardening [3]. Robot laser hardening [4] with an overlapping laser beam is particularly interesting. The result is, of course, an approximation, which is calculated by the desired number of places.

In this paper, fractal analysis is used to determine how parameters of robot laser hardening affect the hardness of the hardened material. Robot laser surface hardening heat treatment [5-6] is complementary to conventional flame or inductive hardening. The energy source for laser hardening is the laser beam, which heats up very quickly, and works on the metal surface area of points up to 1.5 mm and a hardness of 65 HRC. Laser hardening is a process of projecting features, such as non-controlled energy intake, high-performance constancy and an accurate positioning process. A hard martensitic microstructure provides improved surface properties, such as wear resistance and high strength [7-8]. Fractal analysis [9-10] is useful when classical geometry cannot be sufficiently useful to precisely describe the results of irregular facilities. A profound feature of fractals is the fractal dimension D [11-13], which provides an important view of the physical properties of various materials.

This article describes the fractal structure [14] of robot laser-hardened tool steel. Fractal patterns have been found in different mechanical properties of hardened materials (Mandelbrot 1982, Feder 1988). Fractal features have also been observed in mechanical computer simulations, which can be explained by Gauss-Marc fractal random fields. In this work, we have used a scanning electronic microscope (SEM) [15-16] to research for and analyse the fractal structure of robotic laser-hardened material. The aim of the research is to ascertain how robotic laser cell parameters for optimal tempering affect the fractal dimension of hardened material.

2. Experimental method and materials preparation

The study was undertaken using tool steel standard label DIN standard 1.7225. The chemical composition of the material was 0.38-0.45 % C, maximum of 0.4 % Si, 0.6-0.9 % Mn, maximum of 0.025 % P, maximum of 0.035 % S, and 0.15-0.3 % Mo. The specimen test section was in a cylindrical form with dimensions of 25×10 mm. After hardening, the test specimen was cut into smaller parts. Tool steel was forged with a laser at different speeds and at different powers. So we changed the two parameters: speed v was set to 2-5 mm/s in steps of 1 mm/s, and temperature T to 1000-1400 °C in steps of 50 °C. During all these tests, we recorded the microstructure.

We recorded the hardened surface area as well as the deep hardened zone of the clips. Of interest to us was whether the robotic laser hardening parameters for different fractal structures found microparticles. Also, we wanted to know or ascertain the fractal structure of the optimal parameters of hardening. Fig. 1 shows the longitudinal and transverse cross section of hardened tool steel. In Figs. 2, 3, 4, and 5 the microstructures of tempered tool steel at different magnifications are shown.

Fig. 1 Hardened tool steel

Prior to testing, the specimens were subjected first to mechanical and then to electrolytic polishing [17] in H_3PO_4 + CrO_3 at the IMT Institute of Metals and Technology, Ljubljana, Slovenia. After polishing we made images with a microscope. First, we made recordings using an optical microscope and then with an electron microscope. Images were made using a JEOL JSM-7600F field emission scanning electron microscope. Irregular surface textures with a few breaks, represented by black islands, were revealed (Fig. 2).
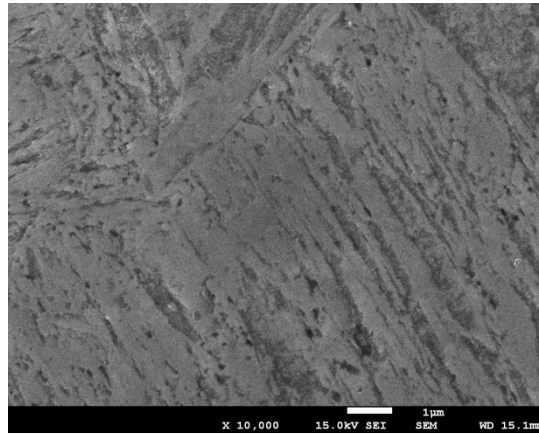
Fig. 2 SEM image of 1000 °C and 2 mm/s at 50000× magnification on the surface
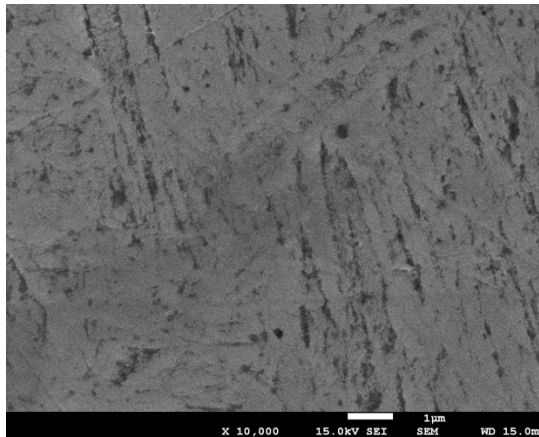
Fig. 3 SEM image of 1400 °C and 5 mm/s at 10,000× magnification on the surface
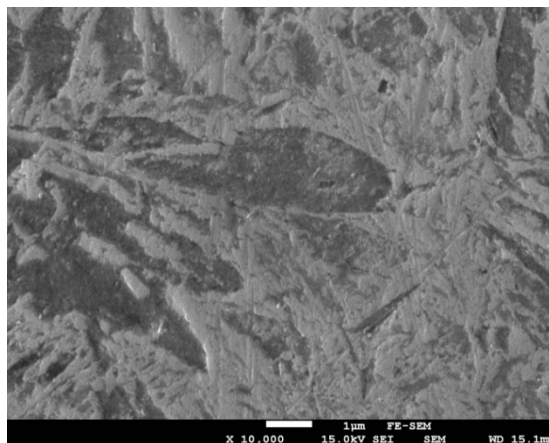
Fig. 4 SEM image of 1000 °C and 3 mm/s at 5000× magnification on the depth
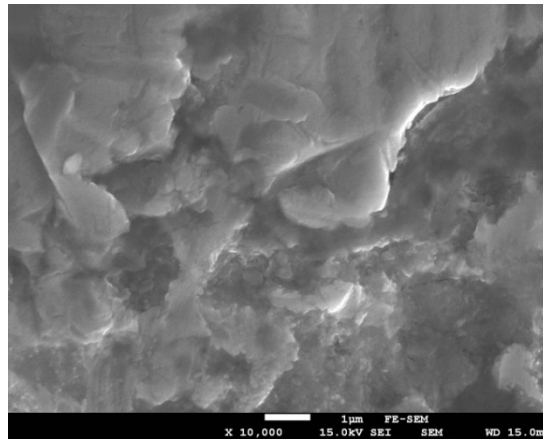
Fig. 5 SEM image of 1400 °C and 2 mm/s at 10000× magnification on the depth

3. The concept of fractals

When analysing the fractal dimensions, we used the R/S method. The R/S method (adjusted rescaled range method) or the adjusted scale is a graphical method and was selected for the estimation of the Hurst exponent. Hurst, the discoverer of the exponent that bears his name, studied power laws as they related to the Nile river floods. The adjusted scale of the partial summation area space component series deviates from the mean. Following Feder, the R/S analysis is as follows. Let the time series of natural phenomena in discrete time in the space component period τ be $\{x_1, x_2,..., x_n\}$. The calculation of the average distance m for the period t is presented in Eq. 1.

$$m = \frac{1}{n} \sum_{u=1}^{n} X_i \tag{1}$$

$Z(t)$ calculates as in Eq. 2.

$$Z(t) = \sum_{u=1}^{t} (X_i - m) \tag{2}$$

$R(n)$ calculates as in Eq. 3.

$$R(n) = \max(Z_1, Z_2, \ldots, Z_n) - \min(Z_1, Z_2, \ldots, Z_n) \tag{3}$$

$S(n)^2$ calculates as in Eq. 4.

$$S(n)^2 = \sum_{u=1}^{t} (X_i - m) \cdot (X_i - m) \tag{4}$$

Hurst observed the relationship R/S for a large number of natural phenomena and found the following empirical relationship in Eq. 5:

$$\frac{R}{S} = (c \, \tau)^H \tag{5}$$

The relationship between Hurst's exponent H and the Box-counting method for determining the fractal dimension D is very simple [10]. It is presented in Eq. 6 (in the plane) and Eq. 7 (in the space).

$$D = 2 - H \tag{6}$$

$$D = 3 - H \tag{7}$$

4. Results and discussions

We analysed the image format (e.g., JPEG) with 256 grey level numerical matrices (level 1 for black and 256 for white) with the program ImageJ. At each point (x, y) in the image (2D plane) the value of 1 to 256 is assigned. This value is then determined by a third coordinate in the 3D coordinate system, or z-coordinate. This means that the point $T = (x, y)$ plane is given by the third component and then forms $T3D = (x, y, z)$. This is presented in Figs. 6, 7, 8, and 9 which show the profile of a hardened specimen with certain parameters on the surface and in the depth. The graph of grey value presents the average of all lines on the y-axis. For each specimen, we have made an image of the microstructure at 5000×, 10,000×, 20,000×, 30,000×, and 50,000× magnification. Then, when we analysed the profile graphs and profiles, we found that the graphs are similar.
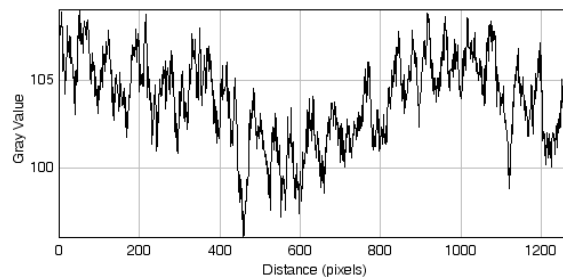
Fig. 6 Profile graph of surface pattern hardened by 2 mm/s at 1000 °C on surface
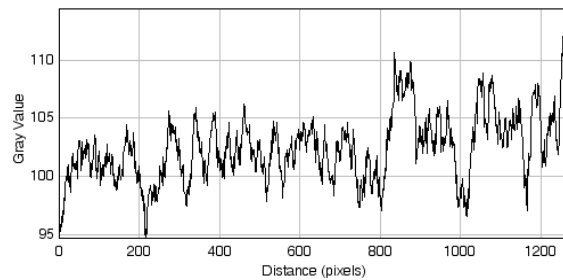
Fig. 7 Profile graph of depth pattern hardened by 3 mm/s at 1000 °C on depth

Comparing the profiles of the graphs we show the fractality of the robot laser-hardened specimens. The comparison is analysed with Hurst parameter H.
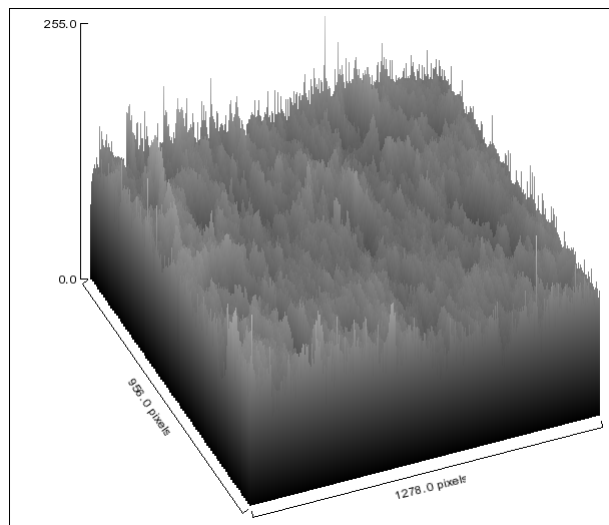
Fig. 8 Three-dimensional graph of the hardened surface of a sample of 2 mm/s at 1000 °C
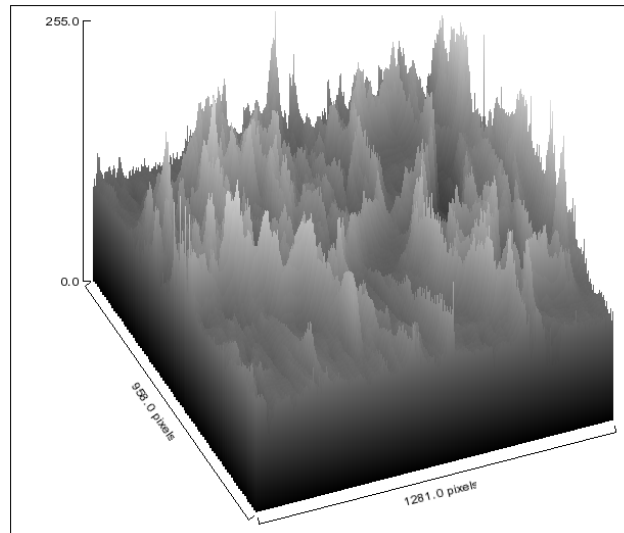
Fig. 9 Three-dimensional graph for of hardened surface of a sample at a depth of 3 mm/s at 1000 °C

For each specimen we calculated the fractal dimension at different magnifications. The results show that the fractal dimension is equal at different magnifications. With this we show the comparison of the microstructures of robot laser-hardened specimens.

Fig. 8 shows an example of the fractal structure of a robot laser-hardened specimen at 1000 °C with 2 mm/s velocity on the surface. Fig. 9 shows an example of the fractal structure of a robot laser-hardened specimen at 1000 °C with a 3 mm/s velocity at depth.

4.1 Influence of parameter temperature of robot laser cell on the fractal dimension

Fig. 10 and Fig. 11 show the relationship between temperature and speed of the robot laser hardening and fractal dimensions on the surface and at depth. If we increase the temperature of the robot laser cell, then the fractal dimension also increases. Fractal dimension is higher on the surface of robot laser hardening patterns. We can see that the fractal dimension decreased in a specimen when we increased the temperature.
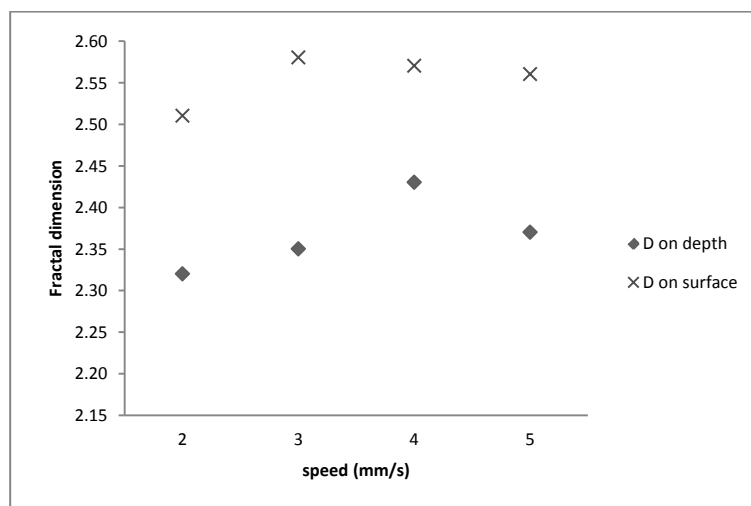
Fig. 10 Fractal dimension at 1000 °C at different speeds of hardening
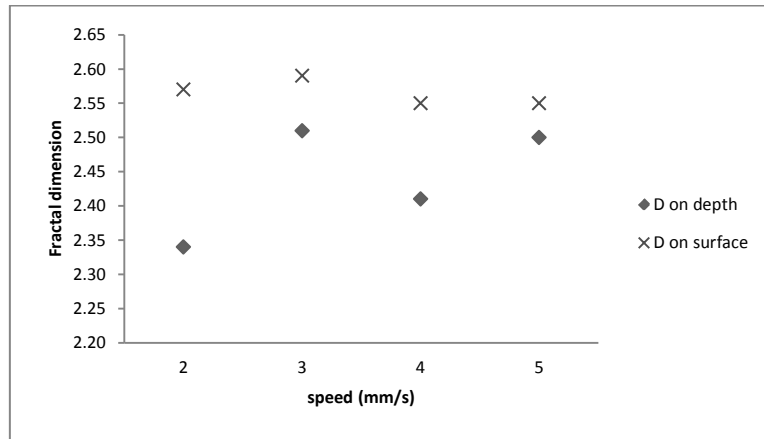
Fig. 11 Dimension at 1400 °C at different speeds of hardening

4.2 Influence of parameter velocity of robot laser cell on the fractal dimension

The speed of the robot laser cell impacts on hardening. We can see that the fractal dimension is higher in depth robot laser-hardened specimens. If we increase the velocity of the robot laser cell then that fractal dimension also increases. This also happens on the depth of robot laser-hardened specimens but differently.

4.3 Fractal dimension and hardness of specimen

Fig. 12 and Fig. 13 present the relationship between fractal dimension and the hardness of specimens hardened with different parameters of the robot laser cell. We can see that the specimen with the least fractal dimension is the hardest.
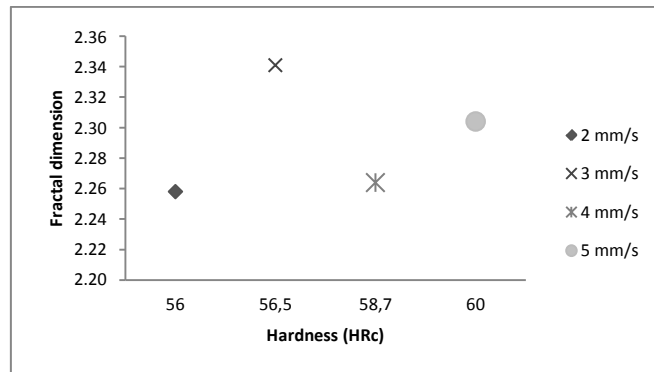
Fig. 12 The fractal dimension at 1000 °C at different speeds depending on hardness
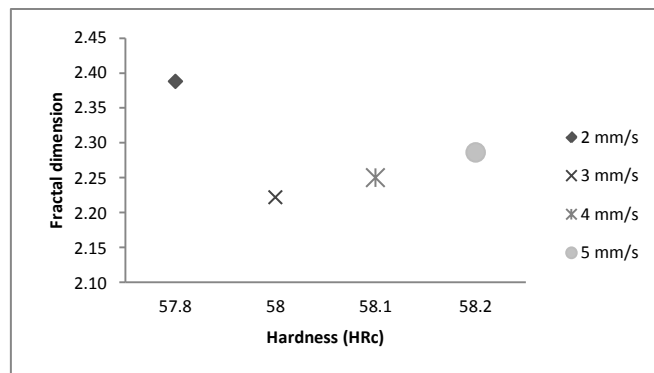
Fig. 13 The fractal dimension at 1400 °C at different speeds depending on hardness

For Fig. 12 and Fig. 13 we calculated the correlation coefficient, showing the size of the linear connection between hardness and fractal dimension. The correlation coefficient for Fig. 12 is $R = 0.0415$. The correlation coefficient for Fig. 13 is $R = 0.2446$. We can see that the correlation coefficients are not similar. Because the correlation coefficients are not 0, the variable hardness and fractal dimensions are correlated. The purpose of this work has been to study how the parameters of robot laser cells impact on the hardness of hardened specimens.

The fractal analysis of a series of digitized surface microstructures from the robot laser surface modified specimens indicated that useful correlations can be derived between the fractal dimensions and the surface microstructural features such as hardness.

5. Conclusion

Fractal structures are also found in robot laser-hardened samples when viewed under sufficient magnification. The hardening of various metal alloys has shown that when melting occurs, fractal geometry can be used to calculate the fractal dimension.

Using the R/S method, we analysed specimens of equal tempered metal after subjecting them to robot laser hardening using various parameters. The main findings can be summarized as follows:

- A fractal structure exists in robot laser hardening.
- The R/S method calculates the fractal dimensions for different parameters of laser hardening robotic cells.
- The optimal fractal dimensions of different parameter robotic laser-hardened tool steel have been identified.
- The fractal dimension varies between 2 and 3. By increasing the temperature of the robot laser cell, the fractal dimension becomes larger and the grain size becomes smaller. Consequently, we can use the fractal dimension as an important factor to define the grain shape.
- The dependence of the fractal dimension on hardness was ascertained. This finding is important if we know that certain alloys mix poorly because they have different melting temperatures, but such alloys have much higher hardness and better technical characteristics. By varying different parameters (temperature and speed), robot laser cells produce different fractal patterns with different fractal dimensions.
- Materials with higher fractal dimensions are less porous than those with lower fractal dimensions.
- Fractal dimension is higher in depth robot laser-hardened specimens.
- Specimens with lower fractal dimensions are the hardest.
- With the correlation coefficients we show a connection between the hardness and the fractal dimension of robot laser-hardened specimens.

The relationship between the microstructure and the parameters of robot laser cells may enable a better understanding of the fractal dimensions by exploring the microstructure.

In the future, we want to explore fractal dimension as a function of the parameters of a robot cell for laser hardening for pinned robot laser hardening: laser parameters such as power, energy density, focal distance, energy density in the focus, focal position, the shape of the laser flash, flash frequency, temperature and speed of hardening. We want to calculate fractal dimensions for different materials to ascertain the relationship between the materials and these parameters of the robot laser cell. We are interested in calculating the fractal dimensions in:

- Two-beam laser robot hardening (where the laser beam is divided into two parts).
- Areas of overlap (where the laser beam covers the already hardened area).
- Robot laser hardening at different angles (where the angles change depending on the x- and y-axes).

Acknowledgement

References

[1] Babič, M., Panjan, P., Kokol, P., Zorman, M., Belič, I., Verbovšek, T. (2013). Using fractal dimensions for determination of porosity of robot laser-hardened specimens, *International Journal of Computer Science Issues*, Vol. 10, No. 2, 184-190.

[2] Mandelbrot, B.B. (1982). *The fractal geometry of nature*, W.H. Freeman and Company, New York.

[3] Babič, M., Milfelner, M., Belič, I., Kokol, P. (2013). Problems associated with a robot laser cell used for hardening, *Materials and Technology*, Vol. 47, No. 1, 37-41.

[4] Vollertsen, F., Partes, K., Meijer, J. (2005). State of the art of laser hardening and cladding, In: *Proceedings of the 3rd International WLT-Conference on Lasers in Manufacturing*, Munich, Germany, 281-305.

[5] Pashby, I.R., Barnes, S., Bryden, B.G. (2003). Surface hardening of steel using a high power diode laser, *Journal of Materials Processing Technology*, Vol. 139, No. 1-3, 585-588, doi: 10.1016/S0924-0136(03)00509-0.

[6] Tesar, J., Vacikova, P., Soukup, O., Houdkova, S. (2012). Infrared camera analysis of laser hardening, *Advances in Optical Technologies*, Vol. 2012, 1-6, doi: 10.1155/2012/593893.

[7] El-Batahgy, A.-M., Ramadan, R.A., Moussa, A.-R. (2013). Laser surface hardening of tool steels – experimental and numerical analysis, *Journal of Surface Engineered Materials and Advanced Technology*, Vol. 3, No. 2, 146-153, doi: 10.4236/jsemat.2013.32019.

[8] Lima, M.S.F., Vasconcelos, G., Riva, R. (2012). Laser surface engineering as a tool for more efficient satellite components, *Journal of Aerospace Engineering, Sciences and Applications*, Vol. 4, No. 4, 105-111.

[9] Feder, J. (1988). *Fractals*, Springer, New York.

[10] Addison, P.S. (1997). *Fractals and chaos: an illustrated course*, Institute of Physics Publishing, London.

[11] Xie, H.P., Liu, J.F., Ju, Y., Li, J., Xie, L.Z. (2011). Fractal property of spatial distribution of acoustic emissions during the failure process of bedded rock salt, *International Journal of Rock Mechanics and Mining Sciences*, Vol. 48, No. 8, 1344-1351, doi: 10.1016/j.ijrmms.2011.09.014.

[12] Li, J., Saharan, A., Koric, S., Ostoja-Starzewski, M. (2012). Elastic-plastic transition in three-dimensional random materials: massively parallel simulations, fractal morphogenesis and scaling functions, *Philosophical Magazine*, Vol. 92, No. 22, 2733-2758, doi: 10.1080/14786435.2012.674223.

[13] Li, J., Ostoja-Starzewski, M. (2014). Fractal shear bands at elastic-plastic transitions in random Mohr-Coulomb materials, *Journal of Engineering Mechanics*, Vol. 140, No. 9, 04014072 (just released), doi: 10.1061/(ASCE)EM.1943-7889.0000750.

[14] Chaudhari, A., Sanders Yan, C.-C., Lee, S.-L. (2004). Multifractal analysis of growing surfaces, *Applied Surface Science*, Vol. 238, No. 1-4, 513-517, doi: 10.1016/j.apsusc.2004.05.247.

[15] Yu, H.-S., Sun, X., Luo, S.-F., Wang, Y.-R., Wu, Z.-Q. (2002). Multifractal spectra of atomic force microscope images of amorphous electroless Ni-Cu-P alloy, *Applied Surface Science*, Vol. 191, No. 1-4, 123-127, doi: 10.1016/ S0169-4332(02)00170-8.

[16] Chen, Z.W., Lai, J.K.L., Shek, C.H. (2005). Multifractal spectra of scanning electron microscope images of SnO_2 thin films prepared by pulsed laser deposition, *Physics Letters A*, Vol. 345, No. 1-3, 218-223, doi: 10.1016/j.physleta.2005.05.104.

[17] Soković, M., Mikuła, J., Dobrzański, L.A., Kopač, J., Koseč, L., Panjan, P., Madejski, J., Piech, A. (2005). Cutting properties of the Al_2O_3 + $SiC_{(w)}$ based tool ceramic reinforced with the PVD and CVD wear resistant coatings, *Journal of Materials Processing Technology*, Vol. 164-165, 924-929, doi: 10.1016/j.jmatprotec.2005.02.071.

Influence of welding speed on the melting efficiency of Nd:YAG laser welding

Tadamalle, A.P.[a,*], **Reddy, Y.P.**[a], **Ramjee, E.**[b], **Reddy, V.K.**[b]

[a]Department of Mechanical Engineering, Sinhgad College of Engineering, Vadgaon, Pune, India
[b]Department of Mechanical Engineering, Jawaharlal Nehru Technological University, Kukatpally, Hyderabad, India

A B S T R A C T

Melting efficiency is one of the more important measurable parameters in laser welding when assessing the performance of a process. This paper aims to study the effects of speed on the melting efficiency and energy transfer efficiency of Nd:YAG laser welding process. The weld bead on a 304L austenitic stainless steel sheet is created by varying the welding speed. The weld samples are cut in the transverse direction by using electric discharge machining, and the cross-section is prepared for metallographic inspection. The cross-sectional dimensions and beads length are measured by using an optical microscope and image analyzer. A methodology is proposed for estimating the weld pool volume from experimental data and a generalised equation for predicting the melting efficiency and energy transfer efficiency is developed. The results obtained by the proposed method have reasonably good agreement with the models proposed by various researchers. The outcome of the result shows the significant influence of welding speed on melting efficiency and energy transfer efficiency in welding of austenitic stainless steel thin sheets. It will be seen from results that one can select appropriate welding speed and processing conditions to obtain desired melting efficiency.

1. Introduction

The Nd:YAG laser welding process is extensively used in modern industrial applications due to increase in demand for micro products. It is very essential to understand the behavior of laser material interaction, controlling of process parameters and their effect on melting, solidification and efficiency. The fundamental figures of merits for the laser welding process can be expressed in terms of melting efficiency, coupling efficiency, process efficiency, and energy transfer efficiency. The other figures of merits considered are fusion zone size, tolerance, and changing base metal temperature. The melting efficiency quantifies the fraction of net heat input to the work piece that is used to produce the weld pool. The absorption of heat by the material is affected by many factors like process parameters, type of laser, incident power density, and base metal surface condition. The optimum melting efficiency and weld strength of the joint depend upon vaporization temperature of the work piece material. The functional characteristics of laser welding process depends upon welding speed, laser power, size of the weld pool geometry, thermal and process efficiencies. The welding efficiency can be improved by fully utilizing the power supplied to melt the unit volume of material.

In literature it has been reported that the effect of very high welding speed on melting efficiency and depth of penetration has been studied [1-2]. The authors discussed the effect of weld-

ing speed on weld bead geometry, and performance parameters such as variation of weld bead diameter from pulse to pulse, duty cycle, and effective pulse energy [3]. The present research work is the continuation of this research on development of new analytical equations to predict the melting efficiency. The experimental and analytical prediction shows that there is a strong dependence of energy absorption on laser power, beam size, and welding efficiency [4-5]. The dimensionless parameters Rykalin (R_y) and Christensen (C_h) are used for computing the melting efficiency of arc and CO_2 laser welding. The melting efficiency of the laser welding process is determined by using experimental results, dimensionless parameter models and energy balance equations. Several researchers have formulated analytical equations to predict the melting efficiency in arc welding process [6-10]. The dimensionless parameter model is very valuable in characterizing partial penetration in laser beam welding process. The material independent model reveals that the variation in laser power and focus spot size is insensitive to the energy transfer efficiency in continuous wave laser beam welding process. A dimensionless parameter model developed for evaluating the melting efficiency in CO_2 laser beam welding has been applied in gas tungsten arc welding (GTAW), plasma arc welding (PAW), and autogenous arc welding processes [11-14].

The energy transfer efficiency of arc and laser welding process is estimated by using calorimetric method and thermal expansion measurement techniques for thin sheets and the results obtained are correlated with the reflection method. The process efficiencies of laser engineered net shaping process is estimated for the tool steel and copper powder material deposits [15-19]. Transient 3D numerical model was developed to study the temperature field and molten pool shape during laser welding and volume of fluid method was employed in the calculations [18]. The influence of welding process parameters, preheating and heat absorption on different laser welding efficiencies is investigated [19-21]. It was found that the global efficiency of the laser welding process decreases slightly by varying the welding speed from 10 mm/s to 2 mm/s, but drops significantly below 1 mm/s [22]. The preheating of weld samples has an effect on absorption efficiency and other efficiencies in the beginning of the process and in the formation of the keyhole [23, 24]. The absorption efficiency and keyhole coupling efficiency are determined by using laser energy reflected from molten pool and by considering plasma effect studied under steady state condition [25].

This paper aims to study the effect of process parameters on melting efficiency (η_m) of Nd:YAG laser weld joints. A semi empirical equation is proposed to estimate the weld pool volume from experimental data, a dimensionless parametric equation to estimate melting efficiency. The section 2 deals with the models proposed by various researchers to evaluate the melting efficiency in different welding process, and section 3 enumerate the experimental procedure adopted. The equations proposed for prediction of weld pool volume and melting efficiency are presented in section 4 and section 5 respectively. The results and discussions are illustrated in section 6 and the conclusions of present work are given in section 7.

2. Melting efficiency

Melting efficiency is defined as the ratio of energy required to create a molten pool from heat energy supplied to the energy absorbed by the work piece. A small percentage of the total energy is used for melting the fusion zone and rest of the energy is dissipated to the surroundings by means of various modes of heat transfer. The literature review reveals that processing parameters, heat flow pattern and thermo-physical properties have significant influence on melting efficiency. A dimensionless parameter model can be used to determine the actual heat input to the metal and the melting efficiency. The dimensionless parameters R_y and C_h are derived from the Rosenthal heat flow solutions. These parameters can be evaluated by using the Eq. 1 developed for the arc welding and CO_2 laser welding process [9]. The Rosenthal heat flow solution model ignores mass additions to the melt pool. Hence modifications are required in the heat flow equations that can incorporate mass addition to the Rosenthal heat flow solution model. However, a semi empirical model can provide reasonable estimates of melting efficiency for both the arc welding and CO_2 laser welding process.

$$C_h = \frac{s^2 A}{\alpha^2} \text{ and } R_y = \frac{P_i s}{\alpha^2 \delta h} \qquad (1)$$

where P_i is the heat input to the substrate (W), α is the thermal diffusivity of base metal (mm²/s), δh is the enthalpy of melting (J/mm³), A is the weld cross-sectional area (mm²), s is the welding speed (mm/s). The melting efficiency (η_m) for the arc welding process [10] can also be expressed as the ratio of dimensionless parameters C_h and R_y [8] as given in Eq. 2.

$$\eta_m = \frac{C_h}{R_y} = \frac{s A \delta h}{\eta_e P_i} \qquad (2)$$

The dimensionless parameter R_y play an important role in estimating the melting efficiency and it is a nonlinear function of heat input and welding speed. Several researchers have developed equations to predict the melting efficiency by using 2D and 3D heat flow conditions. The 2D and 3D heat flow conditions are expressed in terms of thermo-physical properties and processing parameters for predicting the melting efficiency. The mathematical models applied for 2D and 3D heat flow conditions in arc welding process are presented in Eq. 3 and Eq. 4, respectively [10].

$$\eta_m = \frac{1}{\left(\left(\frac{8\,\alpha}{5\,s\,w} \right) + 2 \right)} \qquad (3)$$

$$\eta_m = \frac{1}{1.35 \left(1 + \left(1 + \frac{10.4\,\alpha^2}{(s\,w)^2} \right)^{\frac{1}{2}} \right)} \qquad (4)$$

where w is the bead width (mm). A model applied for predicting the melting efficiency based on power delivered to the substrate material in arc welding process is given in Eq. 5:

$$\eta_m = exp\left(-\left(1 + \frac{\delta h\,\alpha^2}{1.14\,P_i\,s} \right) \right) \qquad (5)$$

In present work, the term power input P_i, supplied by the laser source to the material is replaced by the product of energy transfer efficiency (η_e), voltage (V) and current (I). A semi empirical Eq. 6 is used to predict the melting efficiency based on heat input required to melt the material [7] in GTAW process:

$$\eta_m = \frac{v \int_{T_0}^{T} C_{p(T)} \Delta T + \Delta H_f}{\eta_e t\,P_i} \qquad (6)$$

where ΔH_f is the latent heat of fusion (J/mm³), v is the total volume of melted substrate (mm³), T is the temperature of the weld pool (K), T_0 is the initial temperature (K), t is the laser on time (ms), and C_p is the heat capacity (J/mm³K). The experimental procedure adopted in this work for welding of 304L austenitic stainless steel using Nd:YAG laser welding machine is explained in the next section.

3. Experimental procedure

The welding of 304L austenitic stainless steel sheets is carried out by using pulsed Nd:YAG laser welding machine, TruLaser station 5004 (Trumpf), designed to deliver a maximum laser power of 4 kW. The process parameters, thermo-mechanical properties and chemical composition of 304L stainless steel are given in Table 1 and the setup used for experimentation is shown in Fig. 1. The blank sheets are cleaned before welding by 6-8 % NaOH solution followed by 20 % HNO$_3$ solution. The samples are cut into rectangular specimens of 30 mm by 50 mm with the help of wire cut electric discharge machine to avoid the distortion. The weld quality and aspect ratio of the WBG depends upon welding speed. The threshold value of melting front propagation was found between 1.1-1.4 mm/s and when welding speed is less than 1 mm/s the molten pool irradiates for a longer period of time which results in lower coupling efficiency [22]. The welding speed beyond 10 mm/s does not provide sufficient time to melt the material. Hence, the experiment are planned to conduct on 0.5 mm thick sheet to create a bead on plate by varying the welding speed from 2-10 mm/s in steps of 1 mm/s.
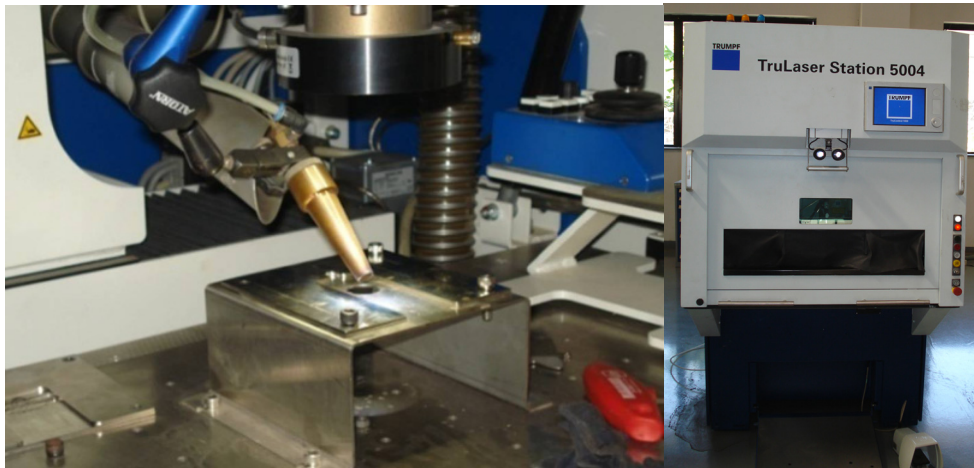
Fig. 1 Specimen mounting arrangement and experimental setup

Table 1 Process parameters and thermo mechanical properties and chemical composition of 304L stainless steel [3]

Process parameters		Thermo mechanical properties of the 304L stainless steel			
Parameters	Values	Parameters	Values	Parameters	Values
Beam diameter	0.4 mm	Density	8030 kg/m^3	Poisons ratio	0.29
Pulse duration	2 ms	Elastic modulus	193 GPa	Melting point	1723 K
Frequency	25 Hz	Mean coefficient of expansion	18.4 μm/m/K	Refractive index	3.81 Fe
Beam angle	90 ± 5 °	Thermal conductivity	20 W/mK	Enthalpy	8.7 J/mm^3
Pulse energy	2.76 J	Specific heat	500 J/kgK	Diffusivity	5.7 mm^2/s

C	Mn	Ni	Cr	Si	V	N	Proof stress	Yield strength	Elongation
0.3	2.0	8-12	18-20	0.75	0.07	0.1	170 MPa	485 MPa	40 %

Table 2 Weld bead geometry dimensions measured from weld samples

Exp. No.	Welding speed (mm/s)	Bead width (μm)	Bead length (μm)	Depth of penetration (μm)
1	2	895	912	500
2	4	845	845	472
3	5	730	730	375
4	7	691	691	233
5	8	687	687	190
6	9	682	682	189
7	10	610	648	100

4. Estimation of weld pool volume

In laser welding process, the selection of preferred levels of welding speed plays an important role to achieve higher melting efficiency. The experiments are conducted by varying welding speed and by keeping all other process parameters constant. The transverse cross-section area, bead length (BL) and bead width (BW) of the weld bead geometry (WBG) are extracted from the samples prepared for metallographic inspection, Fig. 2(a) to Fig. 2(f). The WBG and HAZ profile dimensions are measured by using Metatech (Hitachi) electron microscope. The digitized data obtained from the HAZ profile is used to generate polynomial equations at different welding speeds. This digitized data is best fitted to obtain the second order polynomial equations. A sample second order polynomial equation and corresponding curve obtained from digitized data at a welding speed of 8 mm/s is shown in Fig. 3. Similarly other second order polynomial equations are derived from experiments conducted at different welding speeds. A generalized second order polynomial equation applicable to the geometry of any heat affected zone profile is given in Eq. 7.
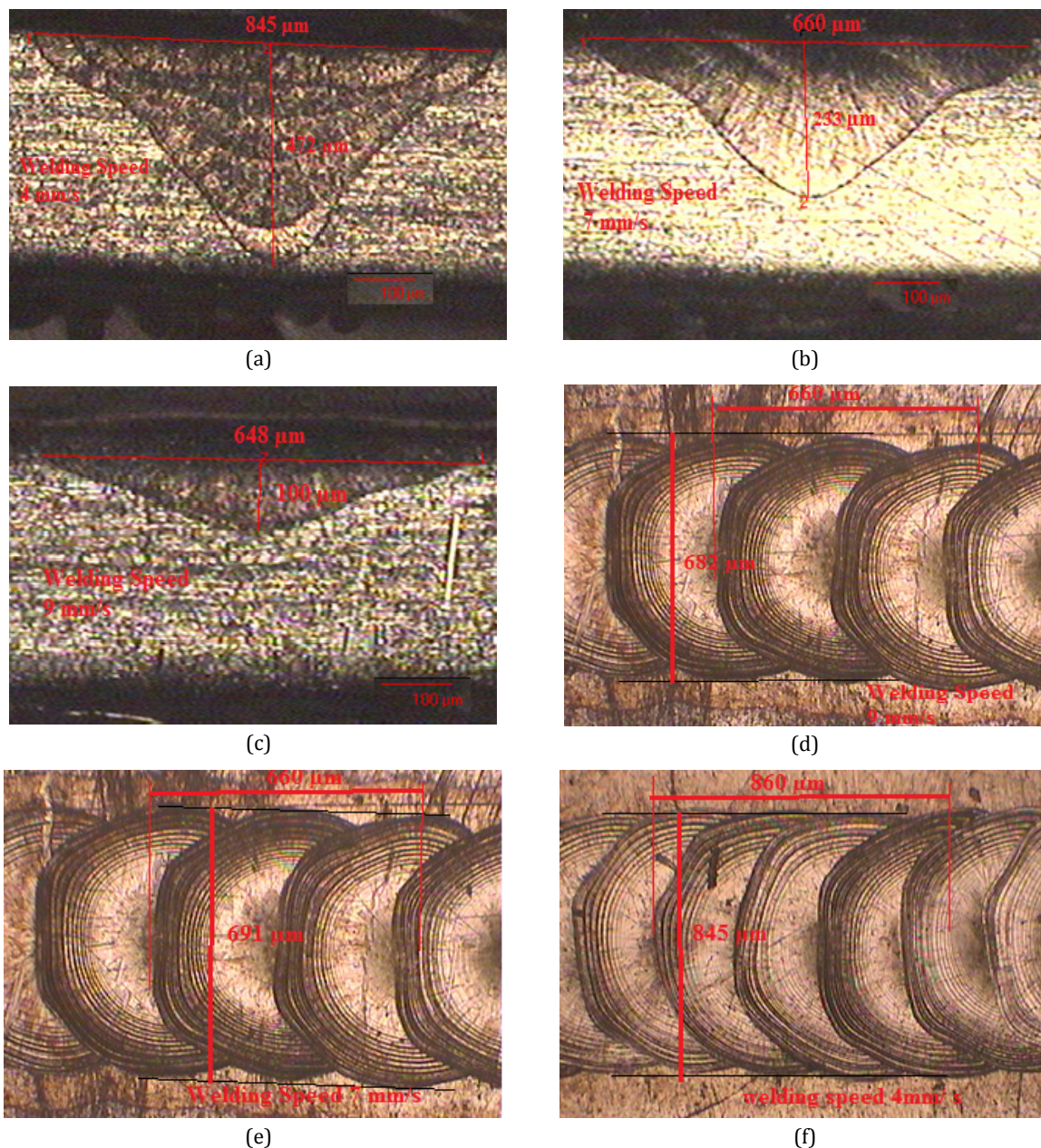
Fig. 2 Samples prepared for metallographic inspection and measurement of WBG
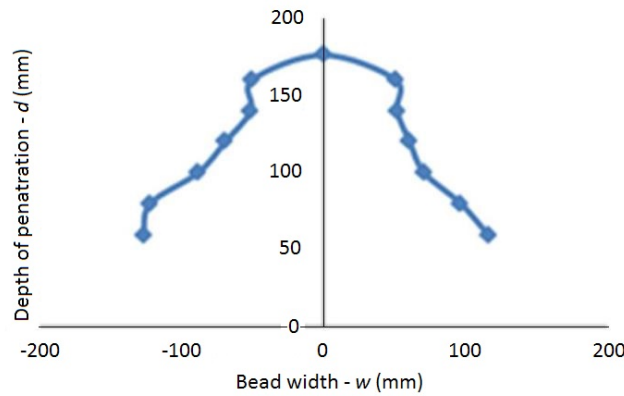
Fig. 3 Digitized data fitted to obtain a second order polynomial equation

$$f(x) = C_1 + C_2 x + C_3 x^2 \tag{7}$$

The coefficients C_1, C_2, and C_3 are constants which are evaluated by using the polynomial equations derived from digitized HAZ data and the variable x denotes the bead width. This data is measured from the cross-sectional view of the micrographs obtained at different welding speeds shown in Table 2. The digitised data is used to obtain a HAZ profile of the weld pool shown in Fig. 3 and the corresponding second order polynomial equation. The weld pool volume estimated by revolving half section of the polynomial curve about the axis of the laser beam is given in Eq. 8.

$$V = \int_0^d (C_1 + C_2 x + C_3 x^2)^2 \, dx \tag{8}$$

A generalized equation proposed to evaluate the weld pool volume by using best fit curve obtained from the geometric mean of all corresponding coefficients.

$$V = 0.512 + 0.028x - 0.007x^2 \tag{9}$$

The weld pool volume and its cross-sectional area is a function of depth of penetration, bead length and bead width. The correct measurement of depth of penetration and bead length is difficult, because it requre metallographic preparation to observe cross-sectional view of the WBG. The bead width can be measured with ease hence it is proposed equation to estimate the weld pool volume in terms of bead width as given in Eq. 10.

$$V = 0.512 + 0.028 \, w - 0.007 w^2 \tag{10}$$

The coefficients given in Eq. 10 are valid in the range of weld speed from 2-10 mm/s. This range is selected because it gives better results in terms of pulse overlapping factor, variation in bead diameter from pulse to pulse and other performance parameters [3] at the specified values of process parameter considered for the study.

5. Prediction of melting efficiency

The dimensionless parameters R_y and C_h can be evaluated by knowing material properties, weld speed, laser power input and weld pool cross-sectional area. The values R_y and C_h are estimated by varying the welding speed and a best fit curve shown in Fig. 4 is obtained by using linear regression analysis technique. The correlation coefficient between C_h and R_y is greater than 0.943 and the relation obtained from the best fit curve is presented in Eq. 11.
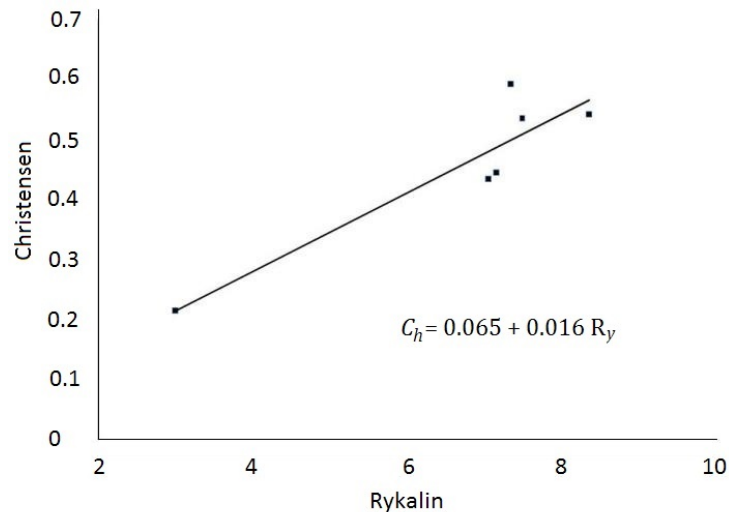
Fig. 4 Relation between Rykalin and Christensen dimensionless parameters

$$C_h = 0.065 + 0.016\,R_y \tag{11}$$

The relationship for melting efficiency (η_m) derived from Eq. 11 is given in Eq. 12:

$$\eta_m = 0.016 + \frac{0.065}{R_y} \qquad \eta_m = 0.065 + 0.016 \left(\frac{\Delta H_m \alpha^2}{\eta_e P_i\, s} \right) \tag{12}$$

The semi empirical Eq. 12 can be used for predicting the melting efficiency of Nd:YAG laser welding process. The melting efficiency is a function of R_y.

The laser beam reflection method is used in this study to estimate energy transfer efficiency. The accurate prediction of weld size is done by considering different values of energy transfer efficiency.

6. Results and discussions

The power absorbed by conduction and melting of the substrate material is more at higher welding speeds. The Fig. 5 reveals that total power absorbed by the substrate material increases with increase in welding speed. This is due to the significant difference in temperature between laser source and work piece material as a result of which more amount of heat is utilized to create and maintain molten weld pool. It is found that the power utilized for melting the material is less than that of power absorbed by conduction up to a welding speed of 7 mm/s. However beyond this limit, power absorbed for creating weld pool is greater than heat carried away by the conduction. This is due to less than 4 ms times is available for transferring heat energy to the substrate material by conduction. The stainless steel material has reflectivity 64 %, whereas for copper, aluminium and nickel it is greater than 74.20 %. Many researchers have determined the melting efficiency in welding by considering energy transfer efficiency constant at 0.37 or 0.48 [7, 10]. In this study, laser beam reflection method is employed to compute energy transfer efficiency.
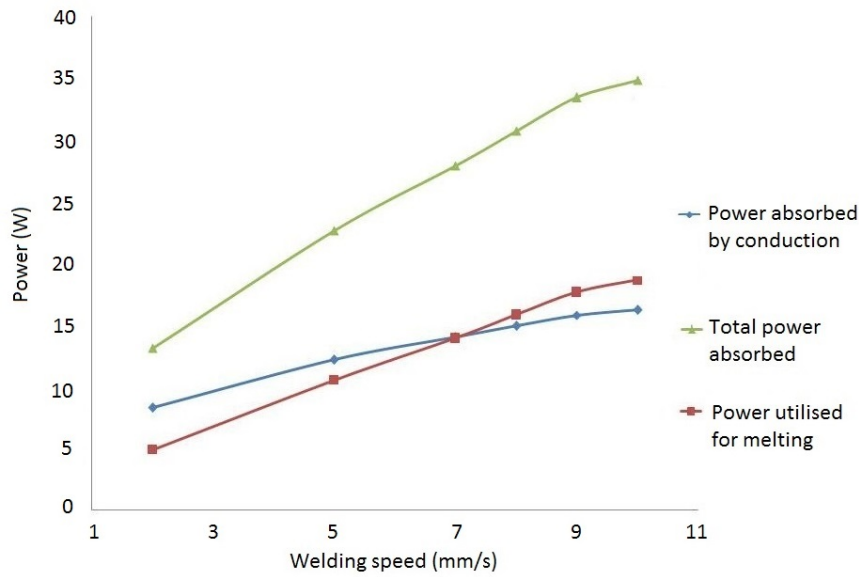
Fig. 5 Effect of welding speed on power absorbed by the specimen

The Fig. 6 shows that there is a significant variation from 10.1-21.2 % in the energy transfer efficiency with respect to welding speed, therefore different values of energy transfer efficiencies are considered instead of a single value.

The heat input to the substrate material is directly proportional to the product of energy supplied, energy transfer efficiency and pulse frequency. The energy transfer efficiency is based on materials properties, laser beam reflection, process parameters, operating conditions and power source. The analytical equations proposed by the researchers to estimate the melting efficiency predict differently for different types of welding processes. A non-linear relationship is observed between the melting efficiency, weld speed, and R_y from the results obtained by different researchers.
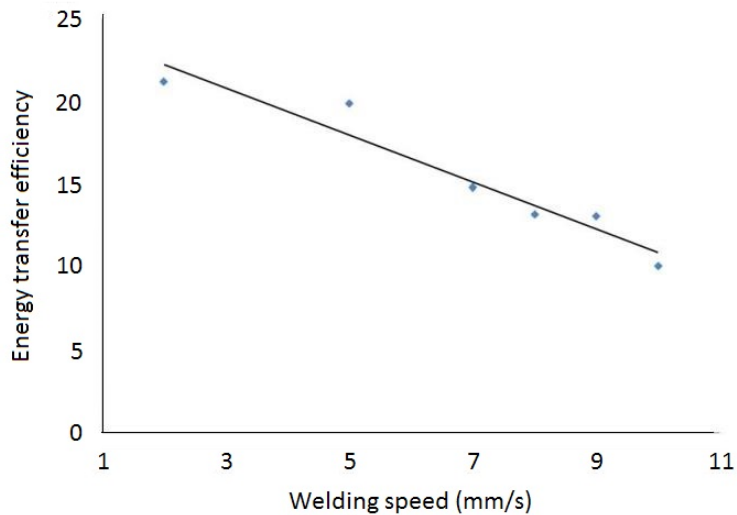
Fig. 6 Correlation between energy transfer efficiency and welding speed
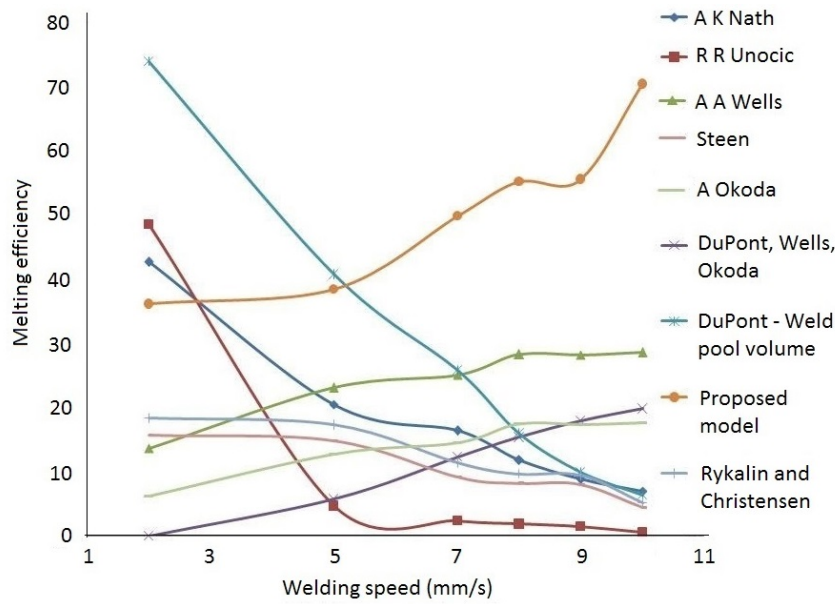
Fig. 7 Comparison of melting efficiencies predicted using proposed models and models presented by different researchers

This is shown in Fig. 7 and Fig. 8. The weld pool volume has been computed by using Eq. 10 and resulting values are substituted to predict melting efficiency. The proposed model predicts higher efficiency than that of other models. This is due to selection of process parameters for dimensionless parameter modeling and the variation in heat energy absorbed by the substrate material with respect to welding speed. It can be seen from Fig. 8: an increase in welding speed leads to increase in melting efficiency. This is because the energy required to melt the substrate material is influenced by welding speed and less time available to transfer heat away from the melt pool region. Hence more amount of energy consumed to create and maintain molten weld pool. The melting efficiency predicted by the proposed models is higher than the other models presented in this paper and are in close agreement [12]. This is due to bead on plate welds be-longs to the 3D heat flow whereas the other models are based on 2D heat flow concepts. The maximum melting efficiency estimated by using the proposed weld pool volume equation and melting efficiency model is 74.20 % and 70.56 %, respectively, at the welding speed of 10 mm/s.
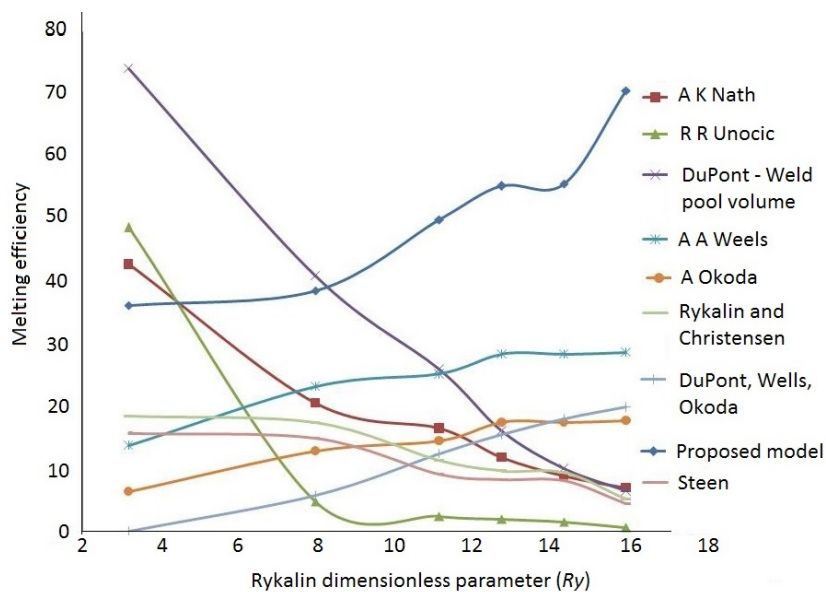
Fig. 8 Comparison of melting efficiencies predicted with respect to Rykalin dimensionless parameter model

7. Conclusion

The melting efficiency of the welding process depends upon processing and operating parameters, thermo mechanical and chemical properties of the material, surface conditions and type of power source. The mathematical model proposed in this work is used to predict weld pool volume by measuring weld bead diameter experimentally and melting efficiency by using dimensionless parameter model. The energy transfer efficiency and melting efficiency are significantly affected by the welding speed. The total power absorbed by the substrate material increases with increasing welding speed. The power utilized for melting the material is less than that of power absorbed by conduction up to a welding speed of 7 mm/s, whereas beyond this limit, power absorbed for creating weld pool is greater than heat carried away by the conduction. The defect free welds have been observed within the range speed selected for welding. The mathematical models presented in this work can be extended for predicting heat flow and solidification modelling studies. The equations developed in this work for estimating melting efficiency predict higher efficiency than the other models. The effect of pulse duration, gas flow rate and focal position on melting efficiency can also be tried. Laser welding at extremely low speeds requires further investigation to explain the reasons behind this drastic change.

Acknowledgement

References

[1] Fuerschbach, P.W., Eisler, G.R. (1999). Effect of very high travel speed on melting efficiency in laser beam welding, *SAE International Journal of Materials and Manufacturing*, Vol. 108, No. 5, 824-829, doi: 10.4271/1999-01-0996.

[2] Lankalapalli, K.N., Tu, J.F., Gartner, M. (1996). A model for estimating penetration depth of laser welding processes, *Journal of Physics D: Applied Physics*, Vol. 29, No. 7, 1831-1841, doi: 10.1088/0022-3727/29/7/018.

[3] Tadamalle, A.P., Reddy, Y.P., Ramjee, E. (2013). Influence of laser welding process parameters on weld pool geometry and duty cycle, *Advances in Production Engineering & Management*, Vol. 8, No. 1, 52-60, doi: 10.14743/apem2013.1.153.

[4] Walsh, C.A. (2002). Laser welding – literature review, Materials Science and Metallurgy Department, University of Cambridge, England, from *http://www.msm.cam.ac.uk/phase-trans/2011/laser_Walsh_review.pdf*, accessed August, 21, 2014.

[5] Pépe, N., Egerland, S., Colegrove, P.A., Yapp, D., Leonhartsberger, A., Scotti, A. (2011). Measuring the process efficiency of controlled gas metal arc welding processes, *Science and Technology of Welding & Joining*, Vol. 16, No. 5, 412-417, doi: 10.1179/1362171810Y.0000000029.

[6] Chang, W.S., Na, S.J. (2002). A study on the prediction of the laser weld shape with varying heat source equations and the thermal distortion of a small structure in micro-joining, *Journal of Materials Processing Technology*, Vol. 120, No. 1-3, 208-214, doi: 10.1016/S0924-0136(01)00716-6.

[7] Fuerschbach, P.W., MacCallum, D.O. (1995). Variation of laser energy transfer efficiency with weld pool depth, In: *Proceedings of 14th International Congress on the Applications of Lasers and Electro-Optics*, San Diego, California, USA, 493-497.

[8] Unocic, R.R., DuPont, J.N. (2004). Process efficiency measurements in the laser engineered net shaping process, *Metallurgical and Materials Transactions B*, Vol. 35, No. 1, 143-152. doi: 10.1007/s11663-004-0104-7.

[9] Fuerschbach, P.W. (1995). A dimensionless parameter model for arc welding process, In: *Trends in Welding Research: Proceedings of the 4th International Conference*, Gatlinburg, Tennessee, USA, 493-497.

[10] DuPont, J.N., Marder, A.R. (1995). Thermal efficiency of arc welding processes, Supplement to the Welding Journal, 406-416, from *http://www.aws.org/wj/supplement/WJ_1995_12_s406.pdf*, accessed August 21, 2014.

[11] Fuerschbach, P.W., Eisler, G.R. (2002). Effect of laser spot weld energy and duration on melting absorption, *Science and Technology of Welding and Joining*, Vol. 7, No. 4, 241-246, doi: 10.1179/136217102225004293.

[12] Nath, A.K., Sridhar, R., Ganesh, P., Kaul, R. (2002). Laser power coupling efficiency in conduction and keyhole welding of austenitic stainless steel, *Sadhana*, Vol. 27, No. 3, 383-392, doi: 10.1007/BF02703659.

[13] Tzeng, Y.-F. (2000). Process characterisation of pulsed Nd:YAG laser seam welding, *The International Journal of Advanced Manufacturing and Technology,* Vol. 16, No. 1, 10-18, doi: 10.1007/PL00013126.

[14] Christensen, N., Davies, V. de L., Gjermundsen, K. (1965). Distribution of temperature in arc welding, *British Welding Journal*, Vol. 12, No. 2, 54-75.

[15] Klimpel, A., Rzeźnikiewicz, A., Janik, Ł. (2007). Study of laser welding of copper sheets, *Journal of Achievements in Materials and Manufacturing Engineering*, Vol. 20, No. 1-2, 467-470.

[16] Norris, J.T., Robino, C.V., Perricone, M.J., Hirschfeld, D.A. (2010). Development of a time-resolved energy absorption measurement technique for laser beam spot welds, *Welding Journal*, Vol. 89, No. 4, 75s-81s.

[17] Wang, R., Lei, Y., Shi, Y. (2011). Numerical simulation of transient temperature field during laser keyhole welding of 304 stainless steel sheet, *Optics & Laser Technology*, Vol. 43, No. 4, 870-873, doi: 10.1016/j.optlastec.2010.10.007.

[18] Patschger, A., Bliedtner, J., Bergmann, J.P. (2013). Approaches to increase process efficiency in laser micro welding, *Physics Procedia*, Vol. 41, 592-602, doi: 10.1016/j.phpro.2013.03.121.

[19] Bergmann, J.P., Patschger, A., Bastick, A. (2011). Enhancing process efficiency due to high focusing with high brightness lasers – applicability and constraints, *Physics Procedia*, Vol. 12, Part A, 66-74, doi: 10.1016/j.phpro.2011.03.009.

[20] Mladenov, G., Vutova, K., Wojcicki, S. (1998). Experimental investigation of the weld depth and thermal efficiency during electron beam welding, *Vacuum*, Vol. 51, No. 2, 231-233, doi: 10.1016/S0042-207X(98)00165-1.

[21] Kim, T.H., Albright, C.E., Chiang, S. (1990). The energy transfer efficiency in laser welding process, *Journal of Laser Applications*, Vol. 2, No. 1, 23-28, doi: 10.2351/1.4745249.

[22] Tu, J.F., Paleocrassas, A.G. (2010). Low speed laser welding of aluminium alloys using single-mode fiber lasers, In: Stone, X.A. (ed.), *Laser Welding*, InTech, 47-76, doi: 10.5772/9857.

[23] Forsman, T., Powell, J., Magnusson, C. (2001). Process instability in laser welding of aluminum alloys at the boundary of complete penetration, *Journal of Laser Applications*, Vol. 13, No. 5, 193-198, doi: 10.2351/1.1404414.

[24] Hamadi, O.A., Khashan, K.S. (2008). Modeling of the preheating effect on keyhole laser welding efficiency, *Iraqi Journal of Applied Physics Letters*, Vol. 1, No. 1, 10-15.

[25] Greses, J., Barlow, C.Y., Hilton, P.A., Steen, W.M. (2003). Effects of different gas environments on CO_2 and Nd:YAG laser welding process efficiencies, In: *SPIE Proceedings: First international Symposium on High-Power Laser Macroprocessing,* Osaka, Japan, 257-263, doi: 10.1117/12.486500.

Scheduling optimization of a flexible manufacturing system using a modified NSGA-II algorithm

Nidhiry, N.M.[a,*], **Saravanan, R.**[b]

[a]Department of Mechanical Engineering, Karapagam University, Coimbatore, Tamil Nadu, India
[b]Department of Mechanical Engineering, Sri Krishna College of Technology, Coimbatore, Tamil Nadu, India

A B S T R A C T

The Flexible Manufacturing System (FMS) belongs to the class of production systems in which the main characteristic is the simultaneous execution of several processes and sharing a finite set of resources. Nowadays, FMS must attend to the demands of market needs for personalized products. Consequently the life-cycle of a product tends to be shorter and a greater variety of products must be produced in a simultaneous manner. The FMS considered in this work has 16 CNC machine tools for processing 80 varieties of products. Since the minimizing of a machine's idle time and thus the minimizing of total penalty costs are contradictory objectives, the problem has a multi-objective nature. The objective of this research was to develop a modified non-dominated sorting genetic algorithm (NSGA-II) for multi-objective optimization. The research will then evaluate and discuss the performance of the modified NSGA-II against the original NSGA-II. The existing NSGA II has been modified in order to improve the global optimal front and reduce the computational effort. The result has been compared with the existing NSGA-II, cuckoo search (CS), particle swarm optimization algorithm (PSO), etc. and it was found that the proposed approach was superior.

1. Introduction

FMS operational decisions consist of pre-release and post-release decisions. FMS planning problems also known as pre-release decisions take into account the pre-arrangement of parts and tools before the operation of FMS begins. The problem of scheduling of FMS, which come under the category of post release decisions deal with the sequencing and routing of the parts when the system is in operation. The problem of loading of machine in an FMS is specified so as to assign the machine, operations of selected jobs, and the tools necessary to perform these operations by satisfying the technological constraints (available machine time and tool slots constraint) in order to ensure the unbalance of the system is minimum with maximum throughput, when the system is on operation. An attempt has been made to solve the objective function and simultaneously to bring the outcome in close proximity to the real assumption of the FMS environment. There are a number of problems faced during the life cycle of an FMS. These problems are classified into design, planning, scheduling and control problems. In particular, task of scheduling and the control problem during the operation are important owing to the dynamic nature of the FMS such as flexible parts, tools and routings of automated guided vehicle (AGV). Scheduling of operations is one of the most critical issues in the planning and managing of manufacturing processes. The increased use of flexible manufacturing systems (FMS) that effectively

provides a customer with diversified products has created a significant set of operational challenges. The design of these kinds of systems is characterized by massive alternatives of positions and paths of components, while in practice there is always the attempt to minimize the cycle time, dealing with a lot of alternatives in respect to positioning of components and paths' planning.

1.1 Earlier research

During the last three decades much research has been done in this area. Many heuristic algorithms have been developed to generate optimum schedule and part-releasing policies. Most of these algorithms include enumerative procedures, mathematical programming and approximation techniques, i.e. linear programming, integer programming, goal programming, dynamic programming, transportation and network analysis, branch and bound, Lagrangian relaxation, priority-rule-based heuristics, local search algorithms (ITS, threshold algorithm, Tabu search, SA), genetic algorithm (GA), etc. Of these techniques, some are specific to particular objectives, and some are specific to particular instances with respect to time needed for computational.

Guo et al. [1] presented a comprehensive review of genetic algorithm based optimization model for scheduling flexible assembly lines. In this paper a scheduling problem in the flexible assembly line is investigated and a bi-level genetic algorithm to solve the scheduling problem is developed. Tiwari and Vidyarthi [2] proposed a genetic algorithm based heuristic to solve the machine loading problem of a random type FMS. The proposed GA based heuristic determines the part type sequence and the operation machine allocation that guarantee the optimal solution to the problem. In another scheduling paper [3], taking into account only 6 machines and 6 jobs. Kumar, Tiwari and Shankar [4], analyzed ant colony optimization approach (ACO) in FMS scheduling. But ACO algorithm performs better in problem such as traveling sales, the vehicle rooting etc. In previous years most research concerning the AGV scheduling has been focused on development of scheduling algorithms for a single objective such as minimizing of setup cost or minimizing the loading and unloading time. Toker, Kondakci and Erkíp [5] proposed an approximation algorithm for the *n* jobs and *m* machines resource constraint job shop problem. Hoitomt et al. [6] explored the use of the Lagrangian relaxation technique to schedule job shops characterized by multiple non-identical machine types, generic procedure constraints and simple routing considerations. He and Kusiak [7] addressed three different industrial scheduling problems, with heuristic algorithms for each problem. Lee and DiCesare [8] used Petri nets to model the scheduling problems in FMS. Shnits and Sinreich [9] present the development of a multi-criteria control methodology for FMSs. The control methodology is based on a two-tier decision making mechanism. The first tier is designed to select a dominant decision criterion and a relevant scheduling rule set using a rule-based algorithm. In the second tier, using a look-ahead multi-pass simulation, a scheduling rule that best advances the selected criterion is determined. Yu and Greene [10] use a simulation study to examine the effects of machine selection rules and scheduling rules for a flexible multi-stage pull system. Jerald et al. [11] proposed a combined objective scheduling optimization solution for FMS. Saravanan and Noorul had modified the same problem in scatter-search approach of flexible manufacturing systems, but this work is only for 43 parts and few generations. Sankar et al. [12] applied multi-objective genetic algorithm FMS for 16 machines and 43 jobs. The results were better than conventional optimization approaches. Burnwal and Deb [13] took the same problem and improved results using cuckoo search (CS) based approach. Udhayakumar and Kumanan [14] have generated an active schedules and optimal sequence of job and tool that can meet minimum make span schedule for the flexible manufacturing system. Kumar et al. [15] proposed a machine selection heuristic and a vehicle assignment heuristic which are incorporated in the differential evolution approach to assign the tasks, to appropriate machine and vehicle, and to minimize cycle time. There are also many other interesting approaches regarding simulation in FMS [16-19] as-well-as several heuristic and other algorithms [20, 21] which can be used for multi-objective problem solving in real production environment. Many authors have been trying to emphasize the utility and advantages of genetic algorithm, simulated annealing, and other heuristics.

In this work, modified approach has been proposed based on the non-dominated sorting genetic algorithm-II (NSGA-II) for multi-objective optimization of a specific manufacturing envi-

ronment with two objectives [22, 23]. The procedures are applied to relatively large-size problems of up to 80 part varieties passing through 16 different CNC machine centres, and the results are found to be closer to the global optimum sequence.

1.2 The main contribution of the paper

The following are the novel aspects in this paper:

- Two new objective functions are considered separately for minimizing penalty cost and minimizing machine idle time. So the optimization model used in this paper is truly an improved one.
- No literature had considered 80 varieties of products for a particular combination of tools in the tool magazines using 16 machines in 5 flexible manufacturing cells (FMC) minimizing penalty cost and minimizing machine idle time. From the results it is proved that the new approach gave better results when compared to other algorithms.
- This paper has considered the advantages of the evolutionary algorithms MOGA and NSGA-II, and developed a modified NSGA-II algorithm for solving the problem.
- Two normalized functions of weighing objective and average fitness factor are used to select the best optimal solution. They are used only for selecting the best Pareto solution from the non-dominated solutions of Pareto optimal fronts obtained from the proposed evolutionary algorithms.
- A user friendly and general purpose software package has been developed in this work for modified NSGA-II algorithm using .NET language that can be used to obtain the optimal solution for any similar problems.

Our proposed optimization methods have the following advantages:

- A global Pareto optimal solution is possible.
- They are easy to program and implement efficiently when compared to conventional optimization techniques.
- The proposed approach consumes only 50 % time in comparing with NSGA-II and is superior in terms of objective function.
- Moreover, the procedure developed in this work can be suitably modified to suit any kind of FMS with a large number of components and machines.
- They offer Pareto optimal fronts that offer more number of optimal solutions for the user to choose from.

2. Problem descriptions

The problem environment, assumption and aim of the present work are as follows:

1. The FMS considered in this work has a configuration as shown in Fig. 1. There are five flexible machining cells (FMCs), each with two to six computer numerical machines (CNCs), an independent and a self-sufficient tool magazine, one automatic tool changer (ATC) and one automatic pallet changer (APC). Each cell is supported by one to three dedicated robots for intra-cell movement of materials between operations. There is a loading station from which parts are released in batches for manufacturing in the FMS. There is an unloading station where the finished parts are collected and conveyed to the final storage area. There is one automatic storage and retrieval system (AS/RS) to store the work in progress. The five FMCs are connected by two identical automated guided vehicles (AGVs). These AGVs perform the inter cell movements between the FMCs, the movement of finished product from any of the FMCs to the unloading station and the movement of semi-finished products between the AS/RS and the FMCs.
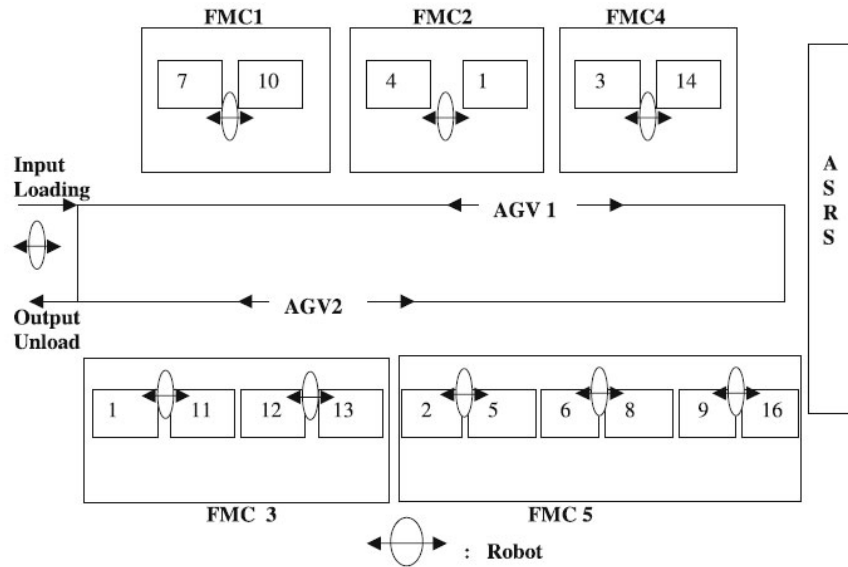
Fig. 1 FMS structure [5]

2. The assumptions made in this work are as follows:

- There are 80 varieties of products for a particular combination of tools in the tool magazines using 16 machines in 5 FMCs.
- The type/variety has a particular processing sequence batch size, deadline and penalty cost for not meeting the deadline.
- Each processing step has a processing time with a specific machine.
- There is no constraint on the availability of pallets, fixtures, AGVs, robots, automated storage and retrieval system, cutting tools, and part programs as and when they are needed at the required places.
- A random product-mix generated as shown in the Table 1 reflect the current market demand.

3. The objective of the schedule:

- Minimizing the machine idle time (TD_i),
- Minimizing the total penalty cost (TP_i).

$$TD_i = \sum_j MI_j \qquad (j - \text{machine number}) \tag{1}$$

$$MI_j = TI - \sum_i PT_{ji} \qquad (i - \text{job number}) \tag{2}$$

$$TP_i = \sum_i (TD_i - DD_i) \times UP_i \times BS_i \tag{3}$$

Nomenclature:

TD_i – Total machine idle time
TI – Total elapsed time
PT_{ji} – Processing time of i-th job on the j-th machine
TP_i – Total penalty cost
PT_i – Processing time of i-th job
DD_i – Due date for i-th job
UP_i – Unit penalty cost for job i
BS_i – Batch size of job i

3. Proposed methodology

As is well-known, a genetic algorithm is a procedure used to find approximate solution to search problems through application of the principles of evolutionary biology. Genetic algorithms uses biologically inspired phenomena such as natural selection, reproduction, crossover and mutation. Genetic algorithms are typically implemented using computer simulations in which an optimization problem is specified.

The two processes together improve an organism's ability to survive with in its environment in the following manner:

- Natural selection determines which organism will have the opportunity to reproduce and survive within a population.
- Reproduction involves genes from two separate individuals combining to form offspring that inherit the survival characteristics of their parents. These algorithms seek to initiate the way in which beneficial gene reproduces themselves through successive population and hence contribute to the gradual ability of an organism to survive.

3.1 NSGA-II algorithm

A multi-objective decision problem is defined as follows. Given an n-dimensional decision variable vector $x = \{x_1,…,x_n\}$ in the solution space X, find a vector x^* that minimizes a given set of K objective functions $z(x^*) = \{z_1(x^*),…,z_K(x^*)\}$. The solution space X is generally restricted by a series of constraints, such as $g_j(x^*) = b_j$ for $j = 1,…,m$, and bounds on the decision variables. Solution to any multi-objective optimization problem is a family of points known as non-dominated solutions or Pareto optimal set, where each objective component of any point along the Pareto-optimal front can only be improved by degrading at least one of its other objective functions. Pareto optimal front is a curve that joins all Pareto optimal set points. If all objective functions of a solution cannot be improved simultaneously, then that solution is said to have non-domination character.

The methodology used to find the optimal solution to this problem is NSGA-II. It is based on a ranking procedure, consisting in extracting the non-dominated solutions for a population and giving them a rank of 1. These solutions are removed from this population; the next group of non-dominated solution has a rank of 2 and so on. The algorithm has a current population that is used to create an auxiliary one (the offspring population); after that, both populations are combined to obtain the new current population. The procedure is as follows: the two populations are sorted according to their rank, and the best solutions are chosen to create the new population. In the case of having to select some individuals with same rank, a density estimation based on measuring the crowding distance to the surrounding individuals belonging to the same rank is used to get the most promising solutions. Typically, both the current and auxiliary population has equal size.
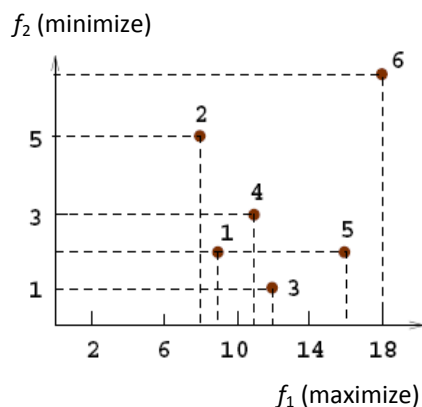
Fig. 2 Values of two objective functions [17]
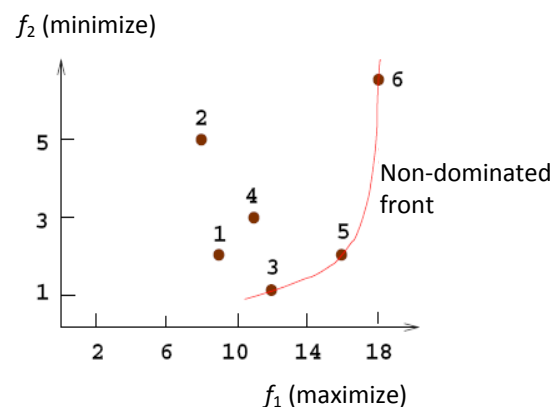
Fig. 3 Pareto-optimal solutions [17]

The concept of dominance is as follows: X_1 dominates X_2 only if X_1 is no worse than X_2 in all objectives, and X_1 is strictly better than X_2 in at least one objective. For example, for two objective functions in Fig. 2, the Pareto-optimal solutions (i.e., non-dominated front) are in Fig. 3. It can be seen that solution 3 dominates solution 2, but it does not dominate solution 5.

3.2 Modified NSGA-II algorithm

The methodology used in this problem is a modified NSGA-II approach to find the optimal solution. The simple GA is modified as a multi objective optimization by including combined objective function (average fitness factor) and non-dominance concept that is used in NSGA-II which is given in the flowchart shown in Fig. 4. After every cycle using combined objective function, new set of solutions is originated. The product sequence obtained after every 500 generations will take and apply NSGA-II algorithm. Then few sequences will be generated with zero dominance count. A new set of optimum solutions will be obtained after 4500 generations.
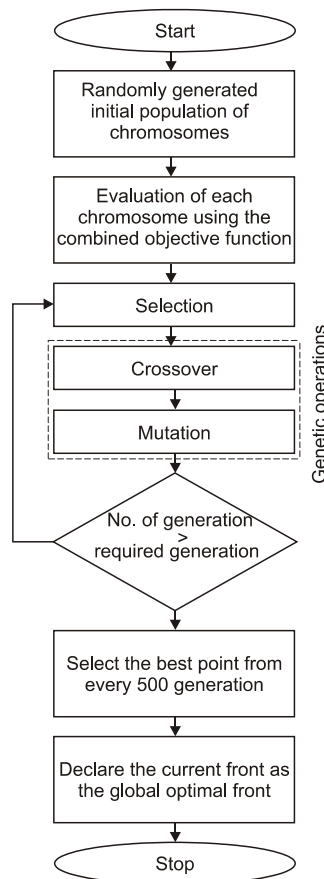
Fig. 4 Flow chart of a modified NSGA-II

3.3 Optimization procedure

Let us suppose the current market demand (Table 1). The objective of the schedule is to minimize the machine idle time (TD_i) and the total penalty cost (TP_i). Combined objective function (COF) is:

$$Objective(1) = \frac{TD_i - Min.TD_i}{Max.TD_i - Min.TD_i} \qquad (4)$$

$$Objective(2) = \frac{TP_i - Min.TP_i}{Max.TP_i - Min.TP_i} \qquad (5)$$

$$Average\ fitness\ factor = \frac{Objective(1) + Objective(2)}{2} \qquad (6)$$

Table 1 Machining sequence, time, deadline, batch size, and penalty details

Part No.	Processing sequence – {Machine No., Processing time (min)}	Deadline (days)	Batch size (Nos)	Penalty cost (INR/unit/day)
1	{6, 1}, {7, 1}, {8, 1}, {10, 2}	17	150	1.00
2	{2, 1}, {6, 1}, {8, 1}, {9, 2}, {14, 4}, {16, 2}	17	200	1.00
3	{8, 1}, {11, 3}, {13, 4}	14	800	1.00
4	{9, 4}	26	700	2.00
5	{4, 5}, {5, 3}, {15, 4}	11	150	1.00
6	{6, 5}, {14, 1}	16	700	1.00
7	{3, 5}, {6, 3}, {16, 5}	26	250	2.00
8	{5, 4}, {6, 5}, {8, 1}	26	850	2.00
9	{4, 1}, {5, 5}, {8, 1}, {11, 1}	1	100	0.00
10	{2, 2}, {9, 1}, {16, 4}	20	150	2.00
11	{8, 4}, {12, 2}	1	250	1.00
12	{6, 2}, {8, 4}, {10, 1}	19	1000	3.00
13	{6, 1}, {7, 5}, {10, 4}	25	700	4.00
14	{4, 2}, {5, 3}, {6, 2}, {15, 2}	22	1000	4.00
16	{5, 3}	27	750	3.00
15	{5, 4}, {8, 3}	15	700	5.00
17	{3, 1}, {6, 4}, {14, 1}	20	650	4.00
18	{9, 2}, {16, 3}	24	250	5.00
19	{4, 1}, {5, 5}, {6, 2}, {8, 2}, {15, 5}	5	450	1.00
20	{8, 2}, {11, 4}	11	50	5.00
21	{4, 5}, {5, 5}, {6, 2}, {8, 2}, {15, 5}	16	850	3.00
22	{12, 5}	24	200	5.00
23	{4, 2}, {5, 1}, {6, 5}, {8, 4}	14	50	4.00
24	{8, 4}, {11, 4}, {12, 5}, {13, 4}	7	200	5.00
25	{7, 3}, {10, 2}	24	350	1.00
26	{10, 2}	27	450	0.00
27	{8, 5}, {11, 5}, {12, 4}	22	400	1.00
28	{2, 1}, {8, 1}, {9, 2}	3	950	5.00
29	{4, 1}, {5, 5}	7	700	1.00
30	{11, 3}, {12, 5}	18	1000	1.00
31	{8, 2}, {10, 2}	2	800	2.00
32	{2, 3}, {6, 4}, {9, 3}	15	800	1.00
33	{5, 4}, {6, 5}, {15, 3}	27	500	4.00
34	{3, 2}, {6, 2}	12	300	4.00
35	{3, 4}, {14, 1}	9	900	2.00
36	{3, 2}	20	700	2.00
37	{1, 5}, {2, 2}, {6, 3}, {8, 3}, {9, 2}, {16, 4}	22	250	4.00
38	{2, 4}, {8, 3}, {9, 2}, {16, 5}	8	50	1.00
39	{6, 5}, {10, 5}	9	500	1.00
40	{2, 2}, {6, 4}, {9, 4}	7	250	5.00
41	{5, 1}, {8, 2}, {15, 1}	22	800	4.00
42	{2, 5}, {6, 4}, {9, 3}, {16,1}	19	400	2.00
43	{1, 3}, {5, 2}, {6, 2}, {8, 2}, {15, 3}	15	550	3.00
44	{2, 5}, {6, 4}, {9, 3}	12	350	1.00
45	{16, 3}, {8, 2}, {2, 3}, {9, 5}	15	400	3.00
46	{1, 3}, {12, 5}, {13, 4}	8	250	4.00

Table 1 Machining sequence, time, deadline, batch size, and penalty details (continuation)

Part No.	Processing sequence – {Machine No., Processing time (min)}	Deadline (days)	Batch size (Nos)	Penalty cost (INR/unit/day)
47	{13, 2}, {12, 3}	7	440	2.00
48	{8, 2}, {16, 3}, {5, 2}	10	350	2.00
49	{1, 3}, {11, 5}	9	300	1.00
50	{16, 2}, {9, 2}, {2, 1}, {6, 3}	8	300	1.00
51	{7, 3}, {10, 2}	20	250	2.00
52	{4, 1}, {1, 2}	16	300	3.00
53	{14, 3}	10	275	4.00
54	{10, 6}, {7, 2}	13	375	2.00
55	{16, 3}, {9, 4}, {6, 2}, {5, 3}	15	220	5.00
56	{13, 2}, {1, 7}, {11, 3}	12	200	3.00
57	{5, 3}, {6, 2}, {9, 3}, {2, 1}	5	150	1.00
58	{7, 5}	7	550	1.00
59	{10, 4}, {7, 8}	8	150	2.00
60	{2, 1}, {9, 3}, {16, 1}	17	500	1.00
61	{1, 6}, {13, 2}, {12, 3}	24	100	2.00
62	{11, 2}, {13, 4}	16	1000	2.00
63	{5, 3}, {2, 11}	18	240	3.00
64	{13, 2}, {11, 3}	27	800	1.00
65	{14, 3}, {3, 11}	19	440	2.00
66	{4, 4}, {1, 3}	14	320	2.00
67	{13, 2}, {1, 3}, {12, 4}, {11, 3}	22	600	4.00
68	{16, 2}, {9, 2}, {8, 1}, {6, 1}	14	700	1.00
69	{8, 1}, {9, 2}, {6, 3}, {5, 3}, {2, 2}	16	150	2.00
70	{7, 5}, {10, 1}	15	230	1.00
71	{3, 14}	7	450	2.00
72	{11, 6}, {12, 10}	18	570	3.00
73	{4, 1}, {1, 5}	9	250	4.00
74	{16, 3}, {9, 2}, {2, 2}	13	200	3.00
75	{16, 1}	3	230	1.00
76	{1, 2}, {5, 3}, {12, 1}	6	310	2.00
77	{2, 2}, {5, 1}, {6, 11}	12	330	3.00
78	{9, 3}, {6, 2}, {5, 3}	14	280	2.00
79	{2, 1}, {9, 3}	14	210	1.00
80	{8, 3}, {9, 3}	10	50	3.00

3.4 GA coding scheme and parameters, genetic operations

As the GA work on coding of parameters, the feasible job sequences (the parameters of the considered problems) are coded in two different ways and separately experimented for the same problem: fino-type coding and binary coding. In this work, fino-type coding is considered. In this coding each sequence is coded as 80 sets of two-digit numbers ranging from 01 to 80.

Example: 60, 54, 20, 79, 18, 45, 49, 72, 27, 41, 59, 34, 50, 32, 25, 29, 31, 2, 37, 69, 43, 21, 71, 67, 46, 64, 6, 63, 19, 56, 74, 17, 15, 42, 35, 65, 1, 68, 52, 26, 7, 24, 57, 10, 75, 80, 28, 66, 36, 9, 13, 3, 4, 5, 30, 12, 16, 70, 55, 77, 76, 11, 14, 53, 48, 51, 58, 8, 22, 33, 73, 61, 62, 40, 44, 23, 78, 39, 47, 38.

GA parameters were:

- Population size: $P = 100$,
- Reproduction: tournament selection (target value – 0.75),
- Crossover probability: $C = 0.6$,
- Mutation probability: $M = 0.01$,
- Termination criteria: 3000 generations or a satisfactory value for objectives, whichever occurs first.

Consider the complexity of one iteration for the entire algorithm. The basic operations and their worst case complexities are as follows: $O(N^{(3/2)} \log N)$, where N is the number of bits in a single chromosome.

Reproduction

The tournament selection method is used for reproduction. Tournament selection is one of many methods of selection in genetic algorithms. Tournament selection involves running several "tournaments" among a few individuals chosen at random from the population. The winner of each tournament (the one with the best fitness) is selected for crossover. Selection pressure is easily adjusted by changing the tournament size. If the tournament size is larger, weak individuals have a smaller chance to be selected. Reproduction procedure is as follows:

- Selection method: tournament selection (assume the parameters for comparison as 0.75).
- Step 1: select two samples from the population.
- Step 2: evaluate the population.
- Step 3: generate random number in the range from 0 to 1.
- Step 4: if the random number is ≤ 0.75, select the best one, else select the inferior one.

Crossover

The strings in the mating pool formed after reproductions are used in the crossover operation (Fig. 5). Single-point crossover is used in this work. With a fino-type coding scheme, two strings are selected at random and crossed at a random site. Since the mating pool contains strings at random, we pick pairs of strings from the top of the list. When two strings are chosen for crossover, first a coin is flipped with a probability $P_c = 0.6$ check whether or not a crossover is desired. If the outcome of the coin flipping is true, the crossover is performed, otherwise the strings are directly placed in the intermediate population for subsequent genetic operation. Flipping a coin with a probability 0.6 is simulated using the Monte Carlo method. The next step is to find a cross site at random. Once crossover point is selected, till this point the permutation is copied from the first parent, then the second parent is scanned and if the number is not yet in the offspring it is added.

$$(\mathbf{1\ 2\ 3\ 4\ 5}\ 6\ 7\ 8\ 9) + (\mathbf{4\ 5\ 3\ 6\ 8}\ 9\ 7\ 2\ 1) = (\mathbf{1\ 2\ 3\ 4\ 5}\ 6\ 8\ 9\ 7)\ (\mathbf{4\ 5\ 3\ 6\ 8}\ 1\ 2\ 7\ 9)$$
$$\quad\text{Parent1}\qquad\qquad\text{Parent2}\qquad\qquad\text{Child1}\qquad\qquad\text{Child2}$$

Fig. 5 Crosssover operation

Mutation

The classic example of a mutation operator involves a probability that an arbitrary bit in a genetic sequence will be changed from its original state (Fig. 6). A common method of implementing the mutation operator involves generating a random variable for each bit in a sequence. This random variable tells whether or not a particular bit will be modified. The purpose of mutation in GAs is to allow the algorithm to avoid local minima by preventing the population of chromosomes from becoming too similar to each other, thus slowing or even stopping evolution. This reasoning also explains the fact that most GA systems avoid only taking the fittest of the population in generating the next but rather a random (or semi-random) selection with a weighting toward those that are fitter. In this work, mutation probability is 0.01, i.e. 8 bits will be mutated. First generate random number from 0 to 1 with accuracy of 0.01. If random number is ≤ 0.01,

then mutation is performed. The next step is to find a cross site at random, the two sites are selected by generating two random numbers between the numbers of jobs. For example, if the random numbers generated are 3 and 6, then the corresponding job numbers in these positions are exchanged.
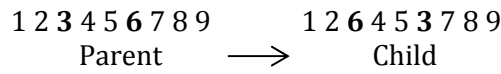
$$1\ 2\ \mathbf{3}\ 4\ 5\ \mathbf{6}\ 7\ 8\ 9 \qquad 1\ 2\ \mathbf{6}\ 4\ 5\ \mathbf{3}\ 7\ 8\ 9$$
$$\text{Parent} \qquad \longrightarrow \qquad \text{Child}$$

Fig. 6 Mutation operation

4. Results and discussions

The optimization procedures developed in this work are based on the modified non-dominated sorting genetic algorithm (NSGA-II). The FMS configuration considered in this work is taken from the literature [11]. In literature, procedure is developed for 43 jobs, using combined objective optimization method. A comparison between the proposed modified NSGA-II and other algorithms namely SPT, PSO, GA, CS [13] (found in literature) and NSGA-II has been presented in Table 2 and Fig. 7. But in this work we have taken the scheduling problem with 80 parts and multi objective optimization approach as well as modified NSGA-II is implemented. The result of modified NSGA-II and existing NSGA-II relating to the problem of 80 jobs are meticulously compared. Table 2 shows the results obtained by the proposed modified NSGA-II. It performs better in terms of objective functions and computational effort, i.e. 50 % less time than the NSGA-II. The Table 3 and Fig. 8 show the comparison of both the approaches in the study. The point in the graph shows the non-dominated points after 4500 generation using NSGA-II and modified NSGA-II.

Table 2 Comparison between various approaches

| Algorithm	SPT [13]	PSO [13]	CS [13]	NSGA-II	Mod. NSGA-II
Machine idle time	180100	315650	163800	109850	95900
Penalty cost	101930	298196	138025	16298	10005
Sequence	20, 23, 38, 1, 9, 26, 22, 10, 34, 18, 36, 11, 25, 5, 16, 2, 40, 4, 41, 31, 7, 24, 28, 17, 6, 29, 35, 37, 15, 39, 42, 27, 33, 3, 43, 19, 13, 12, 32, 30, 8, 14, 21	27, 30, 38, 10, 18, 15, 34, 42, 5, 33, 8, 37, 23, 25, 9, 23, 5, 43, 20, 6, 4, 36, 19, 17, 24, 39, 31, 12, 8, 32, 26, 6, 14, 22, 3, 1, 11, 41, 9, 40, 21, 13, 7	8, 14, 28, 31, 3, 42, 26, 33, 22, 20, 5, 24, 2, 41, 18, 7, 10, 19, 23, 38, 4, 35, 40, 37, 15,17, 39, 6, 2, 34, 1, 29, 27, 16, 36, 30, 25, 32, 13, 3, 11, 10, 9	5, 30, 34, 28, 16, 24, 25, 10, 11, 27, 36, 2, 18, 1, 4, 29, 20, 13, 37, 17, 3, 9, 41, 12, 15, 6, 22, 7, 42, 38, 19, 23, 43, 21, 32, 14, 33, 8, 26, 35, 40, 31, 39	39, 34, 27, 11, 30, 22, 6, 16, 28, 23, 2, 26, 35, 7, 25, 43, 9, 40, 36, 41, 14, 37, 3, 42, 31, 18, 10, 24, 20, 17, 38, 21, 29, 4, 32, 15, 13, 33, 5, 1, 12, 8, 19
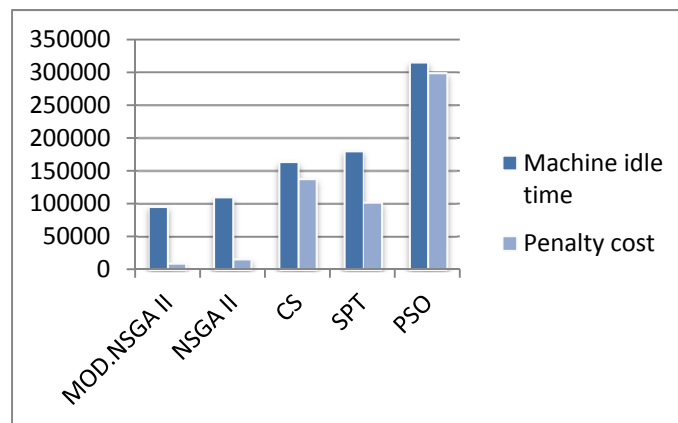
Fig. 7 Comparison between various approaches

Table 3 Results after 3000 generations (80 jobs scheduling problem)

Methodology	Trial No.	Machine idle time (min)	Minimum total penalty cost (INR)
NSGA-II	1	169835	98968.26
	2	167335	99770.35
	3	166415	100289.4
	4	166335	101909.6
	5	160485	108597.4
	6	159565	109116.5
Modified NSGA-II	1	121095	76757.08
	2	121095	76757.08
	3	129815	77308.82
	4	121065	77367.78
	5	121895	77645.97
	6	121895	77645.97
	7	126115	77719.44
	8	121095	77729.31
	9	119875	78162.64
	10	119675	78275.49
	11	127435	78321.32
	12	119545	78347.57
	13	119675	78358.47
	14	123145	78366.67
	15	120465	78409.79
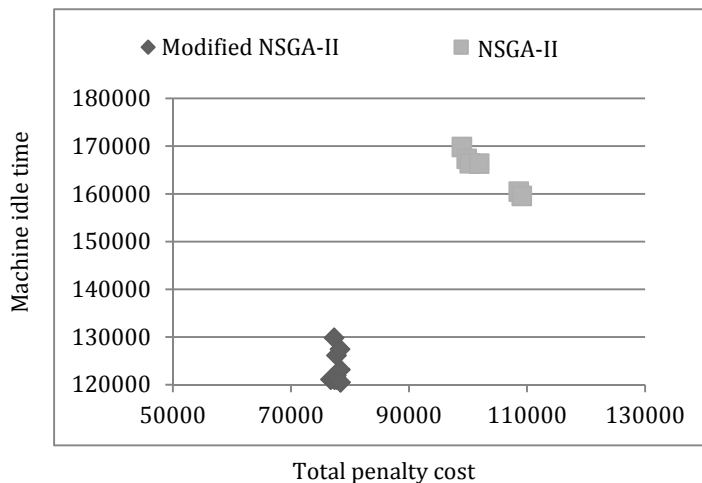
Fig. 8 Comparison of NSGA-II and modified NSGA-II

Results obtained for 80 jobs scheduling problem by modified NSGA-II

Global Pareto optimal front is obtained after executing 4500 generations and the details are shown in Table 4. Results are shown in Fig. 9. The software is executed on an Intel Core 2 Duo based PC with 4 GB RAM using .NET Framework. It took 15 min to complete the computation.

Table 4 Results after 4500 generations (80 jobs scheduling problem)

| Methodology	Trial No.	Machine idle time (min)	Minimum total penalty cost (INR)
Modified NSGA-II	1	116625	73660.42
	2	111625	74692.36
	3	114175	74729.86
	4	114175	74901.74
	5	114175	74901.74
	6	114285	74916.32
	7	111625	75129.86
	8	111325	75207.99
	9	111505	75258.33
	10	114175	75790.63
	11	114175	75811.46
	12	111625	76003.13
	13	111505	76126.39
	14	113025	76270.49
	15	112675	76315.63
	16	114325	76545.83
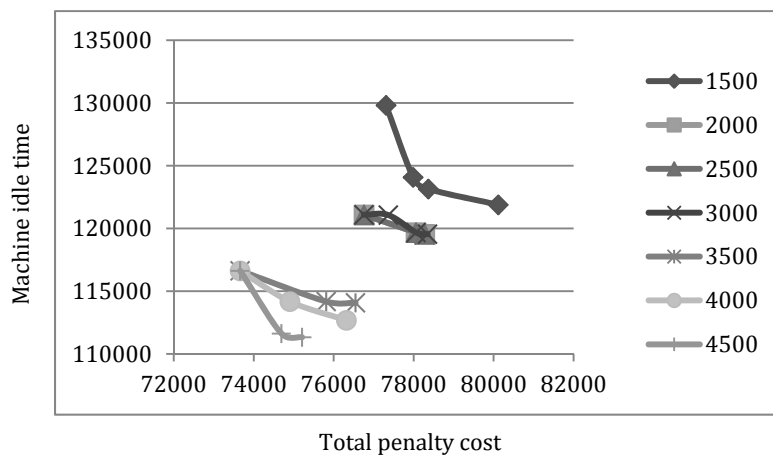
Fig. 9 Progression of Pareto-optimal fronts of modified NSGA-II

5. Conclusion

In this work the optimization procedure has been developed based on the modified multi-objective non-dominated genetic algorithm. This method is implemented successfully for solving the scheduling optimization problem of FMS. Software has been written in the .NET language. FMS schedule is obtained for 80 jobs and 16 machines. The result obtained by modified NSGA-II is analyzed for two objectives, i.e. minimizing total penalty cost and minimizing total machine idle time. After 4500 generation best solution is obtained. The computational effort of FMS scheduling problem is increasing proportional to the number of components. In case of 80 components 7.15694570462638022948115533723187e+118 combinations are possible. Due to very high computational effort exhaustive search is not possible. Similarly random search also requires so much of computational effort. By implementing genetic algorithm for 4500 generations $4.5 \cdot 10^5$ computations needed only for getting the optimal solution. In order to reduce the computational effort further, existing NSGA-II is modified. It is found that the proposed approach consumes 50 % time only in comparing with NSGA-II and is superior in terms of objective function. The procedure developed in this work can be suitably modified to any kind of FMS with a large number of components and machines. Future work will include the availability and handling time of loading and unloading stations, robots and AGV.

References

[1] Guo, Z.X., Wong, W.K., Leung, S.Y.S., Fan, J.T., Chan, S.F. (2008). A genetic-algorithm-based optimization model for scheduling flexible assembly lines, *The International Journal of Advanced Manufacturing Technology*, Vol. 36, No. 1-2, 156-168, doi: 10.1007/s00170-006-0818-6.

[2] Tiwari, M.K, Vidyarthi, N.K. (2000). Solving machine loading problems in flexible manufacturing system using a genetic algorithm based heuristic approach, *International Journal of Production Research*, Vol. 38, No. 14, 3357-3384, doi: 10.1080/002075400418298.

[3] Kumar, A.V.S.S., Veeranna, V., Prasad, B.D., Sarma, B.D. (2010). Optimization of FMS scheduling using non-traditional techniques, *International Journal of Engineering Science and Technology*, Vol. 2, No. 12, 7289-7296.

[4] Kumar, R., Tiwari, M.K., Shankar, R. (2003). Scheduling of flexible manufacturing systems: an ant colony optimization approach, In: *Proceedings of the Institution of Mechanical Engineers, Part B: Journal of Engineering Manufacture*, Vol. 217, No. 10, 1443-1453, doi: 10.1243/095440503322617216.

[5] Toker, A., Kondakci, S., Erkíp, N. (1994). Job shop scheduling under a non-renewable resource constraint, *The Journal of the Operational Research Society,* Vol. 45, No. 8, 942-947, doi: 10.2307/2584018.

[6] Hoitomt, D.J., Luh, P.B., Pattipati, K.R. (1993). A practical approach to job-shop scheduling problems, *Robotics and Automation: IEEE Transactions on*, Vol. 9, No. 1, 1-13, doi: 10.1109/70.210791.

[7] He, W., Kusiak, A. (1992). Scheduling manufacturing systems, *Computers in Industry,* Vol. 20, No. 2, 163-175, doi: 10.1016/0166-3615(92)90050-W.

[8] Lee, D.Y., DiCesare, F. (1994). Scheduling flexible manufacturing systems using Petri nets and heuristic search, *Robotics and Automation: IEEE Transactions on*, Vol. 10, No. 2, 123-132, doi: 10.1109/70.282537.

[9] Shnits, B., Sinreich, D. (2006). Controlling flexible manufacturing systems based on a dynamic selection of the appropriate operational criteria and scheduling policy, *International Journal of Flexible Manufacturing Systems,* Vol. 18, No. 1, 1-27, doi: 10.1007/s10696-006-9001-5.

[10] Yu, M.-C., Greene, T.J. (2006). A simulation analysis of controlling rules for flexible pull systems, *International Journal of Manufacturing Research*, Vol. 1, No. 3, 314-331, doi: 10.1504/IJMR.2006.011961.

[11] Jerald, J., Asokan, P., Prabaharan, G., Saravanan, R. (2004). Scheduling optimisation of flexible manufacturing systems using particle swarm optimisation algorithm, *The International Journal of Advanced Manufacturing Technology*, Vol. 25, No. 9-10, 964-971, doi: 10.1007/s00170-003-1933-2.

[12] Saravana Sankar, S., Ponnanbalam, S.G., Rajendran, C. (2003). A multiobjective genetic algorithm for scheduling a flexible manufacturing system, *The International Journal of Advanced Manufacturing Technology*, Vol. 22, No. 3-4, 229-236, doi: 10.1007/s00170-002-1464-2.

[13] Burnwal, S., Deb, S. (2013). Scheduling optimization of flexible manufacturing system using cuckoo search-based approach, *The International Journal of Advanced Manufacturing Technology*, Vol. 64, No. 5-8, 951-959, doi: 10.1007/s00170-012-4061-z.

[14] Udhayakumar, P., Kumanan, S. (2010). Sequencing and scheduling of job and tool in a flexible manufacturing system using ant colony optimization algorithm, *The International Journal of Advanced Manufacturing Technology,* Vol. 50, No. 9-12, 1075-1084, doi: 10.1007/s00170-010-2583-9.

[15] Kumar, M.V.S, Janardhana, R., Rao, C.S.P. (2011). Simultaneous scheduling of machines and vehicles in an FMS environment with alternative routing*, The International Journal of Advanced Manufacturing Technology,* Vol. 53, No. 1-4, 339-351, doi: 10.1007/s00170-010-2820-2.

[16] Saravanan, M., Haq, A.N. (2008). Evaluation of scatter-search approach for scheduling optimization of flexible manufacturing systems, *The International Journal of Advanced Manufacturing Technology*, Vol. 38, No. 9-10, 978-986, doi: 10.1007/s00170-007-1134-5.

[17] Nakamoto, F.Y., Miyagi, P.E., Santos Filho, D.J. (2008). Resources allocation control in flexible manufacturing systems using the deadlock avoidance method, In: *Proceedings of ABCM Symposium Series in Mechatronics,* Vol. 3, 454-460.

[18] Jian, C.F., Wang, Y. (2014). Batch task scheduling-oriented optimization modelling and simulation in cloud manufacturing, *International Journal of Simulation Modelling*, Vol. 13, No. 1, 93-101, doi: 10.2507/IJSIMM13(1)CO2.

[19] Reddy, B.S.P., Rao, C.S.P (2011). Flexible manufacturing systems modelling and performance evaluation using AutoMod, *International Journal of Simulation Modelling*, Vol. 10, No. 2, 78-90, doi: 10.2507/IJSIMM10(2)3.176.

[20] Deb, K., Pratap, A., Agarwal, S., Meyarivan, T. (2002). A fast and elitist multiobjective genetic algorithm: NSGA-II, *IEEE Transactions on Evolutionary Computation*, Vol. 6, No. 2, 182-197, doi: 10.1109/4235.996017.

[21] Deb, K. (2001). *Multi-objective optimization using evolutionary algorithms*, Wiley, New York, USA.

[22] Nidhiry, N.M., Saravanan, R. (2014). Scheduling optimization of FMS using NSGA-II, *Advances in Industrial Engineering and Management*, Vol. 3, No. 1, 63-72, doi: 10.7508/AIEM-V3-N1-63-72.

[23] Nidhiry, N.M., Saravanan, R. (2014). FMS scheduling optimization using modified NSGA-II, *International Journal of Mechanical and Production Engineering*, Vol. 2, No. 2, 1-6.

Calendar of events

- 2nd International Conference on Industrial and Production Engineering (ICIPE 2014), Chengdu, Kuala Lumpur, Malaysia, September 2-3, 2014.
- International Conference on Manufacturing and Optimization (ICMO 2014), Chengdu, China, September 6-8, 2014.
- 11th International Conference on High Speed Machining, Advances in Manufacturing Technology (HSM 2014), Prague, Czech Republic, September 11-12, 2014.
- ETFA – 2014 IEEE Emerging Technology and Factory Automation, Barcelona, Spain, September 16-19, 2014.
- The 4th International Conference on Industrial Technology and Management (ICITM 2014), Paris, France, September 17-18, 2014.
- 15th International Conference MetalForming 2014, Palermo, Italy, September 21-24, 2014.
- 12th Global Conference on Sustainable Manufacturing (GCSM), Malaysia, September 22-24, 2014.
- 3rd Journal Conference on Innovation, Management and Technology (JCIMT 2014), Geneva, Switzerland, October 10-11, 2014.
- The 15th Asia Pacific Industrial Engineering and Management Systems Conference (APIEMS 2014), Jeju, Republic of Korea, October 12-15, 2014.
- 44th International Conference on Computers & Industrial Engineering (CIE'44), Istanbul, Turkey, October 14-16, 2014.
- 9th International Symposium on Intelligent Manufacturing and Service Systems, Istanbul, Turkey, October 14-16, 2014.
- International Conference on Additive Technologies, Vienna, Austria, October 15-17, 2014.
- 4th International Conference on Advanced Materials and Engineering Materials, Ningbo, Hong Kong, China, October 16-20, 2014.
- 22nd International Conference on Materials and Technology, Portorož, Slovenia, October 20-22, 2014.
- International Conference on Mechatronics, Automation and Manufacturing (ICMAM 2014), Beijing, China, October 24-26, 2014.
- The 16th International Machine Tool Engineers' Conference, Tokyo, Japan, October 31 to November 4, 2014.
- International Conference on Mechatronics and Intelligent Manufacturing (ICMIM 2014), Bahrain, Bahrain, November 5-7, 2014.
- ASME 2014 International Mechanical Engineering Congress & Exposition, Montreal, Canada, November 14-20, 2014.
- METECH' 14 – Innovative Materials and Structures Technologies Metallurgical Engineering Conference, Istanbul, Turkey, November 17-19, 2014.
- 25th DAAAM International Symposium on Intelligent Manufacturing and Automation, Vienna, Austria, November 26-29, 2014.
- The IEEE International Conference on Industrial Engineering and Engineering Management, Selangor/KL, Malaysia, December 9-12, 2014.
- International Conference on Artificial Intelligence and Manufacturing Engineering, Dubai, United Arab Emirates, December 25-26, 2014.
- IEEE International Conference on Industrial Technology, Seville, Spain, March 17-19, 2015.
- IEEE International Conference on Technologies for Practical Robot Applications, Woburn, Massachusetts, USA, May 11-12, 2015.
- IEEE International Conference on Robotics and Automation, Seattle, Washington, USA, May 25-30, 2015.
- IEEE 20th Conference on Emerging Technologies & Factory Automation, Luxembourg, Luxembourg, September 8-11, 2015.

Notes for contributors

General

Articles submitted to the *APEM journal* should be original and unpublished contributions and should not be under consideration for any other publication at the same time. Extended versions of articles presented at conferences may also be submitted for possible publication. Manuscript should be written in English. Responsibility for the contents of the paper rests upon the authors and not upon the editors or the publisher. Authors of submitted papers automatically accept a copyright transfer to *Production Engineering Institute*, *University of Maribor*.

Submission of papers

A submission must include the corresponding author's complete name, affiliation, address, phone and fax numbers, and e-mail address. All papers for consideration by *Advances in Production Engineering & Management* should be submitted by e-mail to the journal Editor-in-Chief:

Miran Brezocnik, Editor-in-Chief
UNIVERSITY OF MARIBOR
Faculty of Mechanical Engineering
Production Engineering Institute
Smetanova ulica 17, SI – 2000 Maribor
Slovenia, European Union
E-mail: editor@apem-journal.org

Manuscript preparation

Manuscript should be prepared in *Microsoft Word 2007* (or higher version) word processor. *Word .docx* format is required. Papers on A4 format, single-spaced, typed in one column, using body text font size of 11 pt, should have between 8 and 12 pages, including abstract, keywords, body text, figures, tables, acknowledgements (if any), references, and appendices (if any). The title of the paper, authors' names, affiliations and headings of the body text should be in *Calibri* font. Body text, figures and tables captions have to be written in *Cambria* font. Mathematical equations and expressions must be set in *Microsoft Word Equation Editor* and written in *Cambria Math* font. For detail instructions on manuscript preparation please see instruction for authors in the *APEM journal* homepage *apem-journal.org*.

The review process

Every manuscript submitted for possible publication in the *APEM journal* is first briefly reviewed by the editor for general suitability for the journal. Notification of successful submission is sent. After initial screening the manuscript is passed on to at least two referees. A double-blind peer review process ensures the content's validity and relevance. Optionally, authors are invited to suggest up to three well-respected experts in the field discussed in the article who might act as reviewers. The review process can take up to eight weeks. Based on the comments of the referees, the editor will take a decision about the paper. The following decisions can be made: accepting the paper, reconsidering the paper after changes, or rejecting the paper. Accepted papers may not be offered elsewhere for publication. The editor may, in some circumstances, vary this process at his discretion.

Proofs

Proofs will be sent to the corresponding author and should be returned within 3 days of receipt. Corrections should be restricted to typesetting errors and minor changes.

Offprints

An e-offprint, i.e., a PDF version of the published article, will be sent by e-mail to the corresponding author. Additionally, one complete copy of the journal will be sent free of charge to the corresponding author of the published article.

APEM
journal

Contents